LA-UR-20-24597 (Accepted Manuscript)

Measurement of the $$ {\Lambda}_b^0 $$ J/ angular distribution and the $$ {\Lambda}_b^0 $$ polarisation in pp collisions

Durham, J. Matthew
Crkovska, Jana
Da Silva, Cesar Luis
Dean, Cameron Thomas
Epple, Eliane Melanie Franziska
Kunde, Gerd Joachim
Li, Xuan
van Hecke, Hubert W.

Provided by the author(s) and the Los Alamos National Laboratory (2020-10-06).

To be published in: Journal of High Energy Physics

DOI to publisher's version: 10.1007/JHEP06(2020)110

Permalink to record: http://permalink.lanl.gov/object/view?what=info:lanl-repo/lareport/LA-UR-20-24597

Disclaimer:
Los Alamos National Laboratory, an affirmative action/equal opportunity employer, is operated by Triad National Security, LLC for the National Nuclear Security Administration of U.S. Department of Energy under contract 89233218CNA000001. By approving this article, the publisher recognizes that the U.S. Government retains nonexclusive, royalty-free license to publish or reproduce the published form of this contribution, or to allow others to do so, for U.S. Government purposes. Los Alamos National Laboratory requests that the publisher identify this article as work performed under the auspices of the U.S. Department of Energy. Los Alamos National Laboratory strongly supports academic freedom and a researcher's right to publish; as an institution, however, the Laboratory does not endorse the viewpoint of a publication or guarantee its technical correctness.

EUROPEAN ORGANIZATION FOR NUCLEAR RESEARCH (CERN)

CERN-EP-2020-051
LHCb-PAPER-2020-005
22 April 2020

arXiv:2004.10563v2 [hep-ex] 25 Jun 2020

Measurement of the $\Lambda_b^0 \to J/\psi\,\Lambda$ angular distribution and the Λ_b^0 polarisation in pp collisions

LHCb collaboration[†]

Abstract

This paper presents an analysis of the $\Lambda_b^0 \to J/\psi\,\Lambda$ angular distribution and the transverse production polarisation of Λ_b^0 baryons in proton-proton collisions at centre-of-mass energies of 7, 8 and 13 TeV. The measurements are performed using data corresponding to an integrated luminosity of $4.9\,\mathrm{fb}^{-1}$, collected with the LHCb experiment. The polarisation is determined in a fiducial region of Λ_b^0 transverse momentum and pseudorapidity of $1 < p_{\mathrm{T}} < 20\,\mathrm{GeV}/c$ and $2 < \eta < 5$, respectively. The data are consistent with Λ_b^0 baryons being produced unpolarised in this region. The parity-violating asymmetry parameter of the $\Lambda \to p\pi^-$ decay is also determined from the data and its value is found to be consistent with a recent measurement by the BESIII collaboration.

Published in J. High Energ. Phys. 2020, 110 (2020)

© 2020 CERN for the benefit of the LHCb collaboration. CC BY 4.0 licence.

[†]Authors are listed at the end of this paper.

1 Introduction

Studies of the production and decay of heavy-flavour hadrons are an important part of contemporary particle physics. The spin-$\frac{1}{2}$ Λ_b^0 baryon can provide information about the production of hadrons containing b quarks. For example, the Λ_b^0 polarisation is closely related to that of the b quark [1]. Heavy-quark effective theory (HQET) predicts that Λ_b^0 baryons originating from energetic b quarks retain a large fraction of the transverse b-quark polarisation [2, 3]. The longitudinal polarisation is expected to vanish in pp collisions due to parity conservation in strong interactions and the term polarisation is used to refer to the transverse polarisation of particles in this paper. The authors of Ref. [4] estimate that the b-quark polarisation is of the order of 10%. This leads to an estimate that the polarisation of the Λ_b^0 baryon can be around 10% with possible values up to 20% [1, 5]. Measurements of Λ polarisation at fixed-target experiments [6–8] find that the polarisation strongly depends on Feynman-x, x_{F}, with polarisation vanishing at $x_{\mathrm{F}} = 0$. The variable x_{F} is defined by $x_{\mathrm{F}} = 2p_{\mathrm{L}}/\sqrt{s}$, where p_{L} is the longitudinal momentum of the baryon with respect to the beam line and $\sqrt{s}$ is the centre-of-mass energy of the collision. If a similar x_{F}-dependence is present in Λ_b^0-baryon production, a negligible polarisation would be expected at the LHC since the experiments mostly cover the phase-space region close to $x_{\mathrm{F}} = 0$. In addition, several heavy b-baryon states are observed experimentally [9–13]. In the production of Λ_b^0 baryons from decays of these states, the connection between the Λ_b^0 and the b-quark polarisation can be further diluted due to the interaction of the b quark with the light quarks in the heavy b-baryon [1, 3]. The fraction of the b-quark polarisation transferred to the Λ_b^0 baryon is estimated to be around 75% in Ref. [1].

The decay $\Lambda_b^0 \to J/\psi\,\Lambda$, where the Λ baryon decays to $p\pi^-$ and the J/ψ meson decays to $\mu^+\mu^-$, can be used to measure the polarisation of the Λ_b^0 baryon as well as to test the theoretical understanding of hadronic decays of Λ_b^0 baryons.[1] The angular distribution of the $\Lambda_b^0 \to J/\psi\,\Lambda$ decay is described by the polarisation of the Λ_b^0 baryon, P_b, four decay amplitudes and by the parity-violating asymmetry parameter of the Λ baryon decay, α_Λ. The decay parameter α_Λ arises due to the V−A nature of the weak interaction [14]. The four decay amplitudes, $A(\lambda_\Lambda, \lambda_{J/\psi})$ correspond to different Λ and J/ψ helicities, λ_Λ and $\lambda_{J/\psi}$. The notation $a_\pm = A(\pm\frac{1}{2}, 0)$ and $b_\pm = A(\mp\frac{1}{2}, \pm 1)$ is used in this paper.

In the naive heavy-quark and light-diquark limit, the u and d quark in the baryon form a spin- and isospin-zero spectator system. The left-handed nature of the charged-current interaction then implies that the Λ-baryon helicity is $-\frac{1}{2}$, such that $|a_+| \approx |b_-| \approx 0$. Several theoretical approaches have been used to predict the Λ_b^0 parity-violating decay parameter

$$\alpha_b = \frac{|a_+|^2 - |a_-|^2 + |b_+|^2 - |b_-|^2}{|a_+|^2 + |a_-|^2 + |b_+|^2 + |b_-|^2}\ , \tag{1}$$

which is the analogue of α_Λ but applied to the Λ_b^0 decay. The value of α_b is predicted to be in the range from −0.2 to −0.1 within a factorisation approximation [15–17], around −0.2 in the covariant oscillator quark model [18] or light-front quark model [19] and in the range from −0.17 to −0.14 in approaches based on perturbative QCD [20]. In contrast, a prediction based on HQET yields a value of $\alpha_b \sim 0.8$ [5]. The covariant quark

[1] The inclusion of charge-conjugate processes is implied throughout this paper except when stated otherwise.

model has recently been used to predict $\alpha_b \sim -0.07$ and the magnitudes of the four helicity amplitudes [21, 22]. The amplitudes predicted by this model agree with the naive expectation that $|a_+|$ and $|b_-|$ are small, while $|a_-|$ and $|b_+|$ are of similar size.

The polarisation of Λ_b^0 baryons was previously measured at LEP in Z decays [23–25] and at the LHC in pp collisions [26, 27]. The values measured at the LHC are

$$P_b = 0.06 \pm 0.07 \pm 0.02 \quad \text{(LHCb)} \ ,$$
$$P_b = 0.00 \pm 0.06 \pm 0.02 \quad \text{(CMS)} \ .$$

Both measurements were performed using an angular analysis of the $\Lambda_b^0 \to J/\psi\,\Lambda$ decay. The LHCb measurement used data collected at $\sqrt{s} = 7\,\text{TeV}$, while the CMS measurement used data from both 7 and 8 TeV pp collisions. A similar analysis was performed by the ATLAS collaboration [28] but assuming $P_b = 0$ and measuring only magnitudes of the decay amplitudes. While all three measurements are compatible, the LHCb and CMS results are unphysical; the LHCb value of $|b_-|^2$ and the CMS value of $|a_+|^2$ are negative. This is likely to be due to the use of a now outdated value of $\alpha_\Lambda = 0.642 \pm 0.013$ from an earlier Particle Data Group average of the results of Refs. [29–33] that is no longer used. This value is significantly smaller than that measured by the BESIII collaboration using $J/\psi \to \Lambda\overline{\Lambda}$ decays [34]. In their analysis, the BESIII collaboration determine α_Λ and $\alpha_{\overline{\Lambda}}$, for the $\Lambda \to p\pi^-$ and $\overline{\Lambda} \to \overline{p}\pi^+$ decays, to be $\alpha_\Lambda = 0.750 \pm 0.009 \pm 0.004$ and $\alpha_{\overline{\Lambda}} = -0.758 \pm 0.010 \pm 0.007$. The BESIII measurement is supported by a reanalysis of CLAS $\gamma p \to K^+\Lambda$ scattering data in Ref. [35], which gives $\alpha_\Lambda = 0.721 \pm 0.006 \pm 0.005$. The polarisation of Λ_b^0 baryons has also been determined to be $P_b = (0 \pm 5)\%$ in the LHCb acceptance using $\Lambda_b^0 \to \Lambda\mu^+\mu^-$ decays, under the assumption that the polarisation is independent of $\sqrt{s}$ [36].

This paper describes a measurement of the $\Lambda_b^0 \to J/\psi\,\Lambda$ angular distribution using data collected with the LHCb experiment during Run 1 and Run 2 of the LHC. The data set corresponds to 1.0, 2.0 and 1.9 fb^{-1} of integrated luminosity collected at $\sqrt{s} = 7$, 8 and 13 TeV in 2011, 2012 and 2015–2016, respectively. A measurement of the polarisation and the decay amplitudes is made, using the BESIII value of α_Λ as an input. The polarisation of Λ_b^0 baryons is measured for the first time at $\sqrt{s} = 13\,\text{TeV}$.

The paper starts by describing the angular formalism used in the analysis in Section 2. Section 3 introduces the LHCb detector. Section 4 describes the selection of candidates from the LHCb data set. The yields of $\Lambda_b^0 \to J/\psi\,\Lambda$ decays in the different data sets are obtained in Section 5. Section 6 describes the procedure used to correct the data for the nonuniformity of the reconstruction and selection. The production polarisation and decay amplitudes are obtained through a two-step procedure described in Sections 7 and 9. Section 8 discusses sources of systematic uncertainty in the measurement. Finally, conclusions are presented in Section 10.

2 Angular formalism

The kinematics of the $\Lambda_b^0 \to J/\psi\,\Lambda$ decay, including the subsequent decays of the J/ψ meson and the Λ baryon, can be parameterised by five decay angles and a unit vector in the direction transverse to the production plane, $\hat{n}$, against which the polarisation is measured [37]. The unit vector is defined as $\hat{n} = (\vec{p}_{\text{beam}} \times \vec{p}_{\Lambda_b^0})/|\vec{p}_{\text{beam}} \times \vec{p}_{\Lambda_b^0}|$, where $\vec{p}_{\Lambda_b^0}$ and $\vec{p}_{\text{beam}}$ are vectors in the direction of the Λ_b^0 baryon and the beam in the centre-of-mass

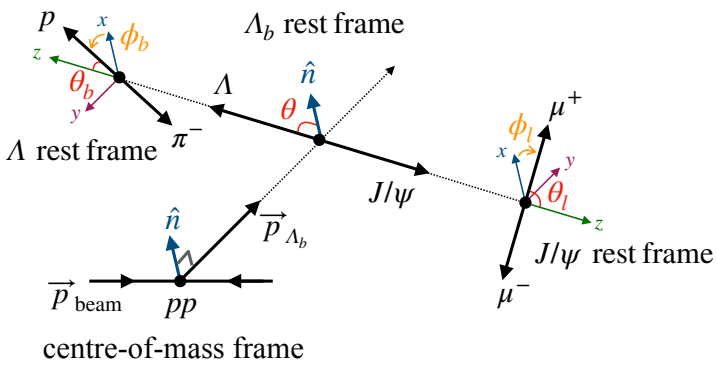

Figure 1: Definition of the five decay angles, θ, θ_b, ϕ_b, θ_l and ϕ_l used to describe the kinematics of the $\Lambda_b^0 \to J/\psi\,\Lambda$ decay. The angles are described in the text.

frame of the pp collision. In the case of the LHCb detector, $\vec{p}_{\text{beam}}$ is the direction of the beam that points into the detector from the collision point. The four-momentum of each particle is boosted into the centre-of-mass frame to account for the small beam-crossing angle of the LHC collisions before $\hat{n}$ is calculated. The five decay angles are: the angle, θ, between $\hat{n}$ and the Λ flight direction in the Λ_b^0 rest frame; the polar, θ_b, and azimuthal, ϕ_b, angles of the proton in the Λ rest frame; and the polar, θ_l, and azimuthal, ϕ_l, angles of the μ^+ in the J/ψ rest frame. The angles θ, θ_l and θ_b are defined in the range $[0, \pi]$, while ϕ_l and ϕ_b are defined over $[-\pi, +\pi]$. A visual depiction of the angular basis is given in Fig. 1. The decay angles for the $\overline{\Lambda}_b^0$ decay are defined assuming no CP violation in the Λ_b^0 or Λ decay, such that the distributions of Λ_b^0 and $\overline{\Lambda}_b^0$ decays are identical.

The angular distribution of the $\Lambda_b^0 \to J/\psi\,\Lambda$ decay can be expressed as [38]

$$\frac{\mathrm{d}^5\Gamma}{\mathrm{d}\vec{\Omega}} = \frac{3}{32\pi^2} \sum_i J_i(a_+, a_-, b_+, b_-, \alpha_\Lambda, P_b) f_i(\vec{\Omega}) \ , \tag{2}$$

where $\vec{\Omega} = (\cos\theta, \cos\theta_b, \phi_b, \cos\theta_l, \phi_l)$. The angular terms, J_i, and the angular functions, f_i, are given in Table 1. The Λ_b^0 polarisation is accessible through terms J_{11}–J_{34}.

3 Detector and simulation

The LHCb detector [39, 40] is a single-arm forward spectrometer covering the pseudo-rapidity range $2 < \eta < 5$, designed for the study of particles containing b or c quarks. The detector includes a high-precision tracking system consisting of a silicon-strip vertex detector surrounding the pp interaction region [41], a large-area silicon-strip detector located upstream of a dipole magnet with a bending power of about 4 Tm, and three stations of silicon-strip detectors and straw drift tubes [42, 43] placed downstream of the magnet. The tracking system provides a measurement of the momentum, p, of charged particles with a relative uncertainty that varies from 0.5% at low momentum to 1.0% at 200 GeV/c. The minimum distance of a track to a primary pp collision vertex (PV), the impact parameter (IP), is measured with a resolution of $(15 + (29\,\text{GeV}/c)/p_{\text{T}})$ μm, where

Table 1: Angular functions parameterising the $\Lambda_b^0 \to J/\psi\,\Lambda$ angular distribution. The numbering scheme is the same as in Ref. [37].

i	J_i	$f_i(\vec{\Omega})$
1	$\frac{1}{4}(2\lvert a_+\rvert^2 + 2\lvert a_-\rvert^2 + \lvert b_+\rvert^2 + \lvert b_-\rvert^2)$	$\sin^2\theta_l$
2	$\frac{1}{2}\lvert b_+\rvert^2 + \frac{1}{2}\lvert b_-\rvert^2$	$\cos^2\theta_l$
4	$\frac{1}{4}\alpha_\Lambda(2\lvert a_+\rvert^2 - 2\lvert a_-\rvert^2 - \lvert b_+\rvert^2 + \lvert b_-\rvert^2)$	$\sin^2\theta_l\cos\theta_b$
5	$\frac{1}{2}\alpha_\Lambda(\lvert b_-\rvert^2 - \lvert b_+\rvert^2)$	$\cos^2\theta_l\cos\theta_b$
7	$\frac{1}{\sqrt{2}}\alpha_\Lambda\mathrm{Re}(-b_+^* a_+ + b_- a_-^*)$	$\sin\theta_l\cos\theta_l\sin\theta_b\cos(\phi_b+\phi_l)$
9	$\frac{1}{\sqrt{2}}\alpha_\Lambda\mathrm{Im}(b_+^* a_+ - b_- a_-^*)$	$\sin\theta_l\cos\theta_l\sin\theta_b\sin(\phi_b+\phi_l)$
11	$\frac{1}{4}P_b(2\lvert a_+\rvert^2 - 2\lvert a_-\rvert^2 + \lvert b_+\rvert^2 - \lvert b_-\rvert^2)$	$\sin^2\theta_l\cos\theta$
12	$\frac{1}{2}P_b(\lvert b_+\rvert^2 - \lvert b_-\rvert^2)$	$\cos^2\theta_l\cos\theta$
14	$\frac{1}{4}P_b\alpha_\Lambda(2\lvert a_+\rvert^2 + 2\lvert a_-\rvert^2 - \lvert b_+\rvert^2 - \lvert b_-\rvert^2)$	$\sin^2\theta_l\cos\theta_b\cos\theta$
15	$-\frac{1}{2}P_b\alpha_\Lambda(\lvert b_+\rvert^2 + \lvert b_-\rvert^2)$	$\cos^2\theta_l\cos\theta_b\cos\theta$
17	$-\frac{1}{\sqrt{2}}P_b\alpha_\Lambda\mathrm{Re}(b_+^* a_+ + b_- a_-^*)$	$\sin\theta_l\cos\theta_l\sin\theta_b\cos(\phi_b+\phi_l)\cos\theta$
19	$\frac{1}{\sqrt{2}}P_b\alpha_\Lambda\mathrm{Im}(b_+^* a_+ + b_- a_-^*)$	$\sin\theta_l\cos\theta_l\sin\theta_b\sin(\phi_b+\phi_l)\cos\theta$
21	$-\frac{1}{\sqrt{2}}P_b\mathrm{Im}(b_+^* a_- - b_- a_+^*)$	$\sin\theta_l\cos\theta_l\sin\phi_l\sin\theta$
23	$\frac{1}{\sqrt{2}}P_b\mathrm{Re}(b_+^* a_- - b_- a_+^*)$	$\sin\theta_l\cos\theta_l\cos\phi_l\sin\theta$
25	$\frac{1}{\sqrt{2}}P_b\alpha_\Lambda\mathrm{Im}(b_+^* a_- + b_- a_+^*)$	$\sin\theta_l\cos\theta_l\cos\theta_b\sin\phi_l\sin\theta$
27	$-\frac{1}{\sqrt{2}}P_b\alpha_\Lambda\mathrm{Re}(b_+^* a_- + b_- a_+^*)$	$\sin\theta_l\cos\theta_l\cos\theta_b\cos\phi_l\sin\theta$
30	$P_b\alpha_\Lambda\mathrm{Im}(a_+ a_-^*)$	$\sin^2\theta_l\sin\theta_b\sin\phi_b\sin\theta$
32	$-P_b\alpha_\Lambda\mathrm{Re}(a_+ a_-^*)$	$\sin^2\theta_l\sin\theta_b\cos\phi_b\sin\theta$
33	$-\frac{1}{2}P_b\alpha_\Lambda\mathrm{Re}(b_+^* b_-)$	$\sin^2\theta_l\sin\theta_b\cos(2\phi_l+\phi_b)\sin\theta$
34	$\frac{1}{2}P_b\alpha_\Lambda\mathrm{Im}(b_+^* b_-)$	$\sin^2\theta_l\sin\theta_b\sin(2\phi_l+\phi_b)\sin\theta$

p_{T} is the component of the momentum transverse to the beam. Muons are identified by a system composed of alternating layers of iron and multiwire proportional chambers [44]. The online event selection is performed by a trigger [45], which consists of a hardware stage, based on information from the muon system and calorimeters, followed by a software stage, which applies a full event reconstruction.

Samples of simulated events are required to model the effects of the detector acceptance and the imposed selection requirements on the $\Lambda_b^0 \to J/\psi\,\Lambda$ angular distribution. In the simulation, pp collisions are generated using Pythia [46] with a specific LHCb configuration [47]. Decays of unstable particles are described by EvtGen [48], in which final-state radiation is generated using Photos [49]. The interaction of the generated particles

with the detector, and its response, are implemented using the GEANT4 toolkit [50] as described in Ref. [51]. The p_{T} distribution of the simulated Λ_b^0 baryons is weighted to match the spectrum observed in Ref. [52].

4 Candidate selection

Signal candidates are formed by combining a J/ψ-meson candidate with a Λ-baryon candidate. The J/ψ candidates are reconstructed from two oppositely charged tracks that have been identified as muons. The muons are required to have a significant IP with respect to all PVs in the event and form a common vertex with a good vertex-fit quality. The dimuon mass is required to be in the range $2900 < m(\mu^+\mu^-) < 3150\,\mathrm{MeV}/c^2$. The Λ candidates are reconstructed in two categories: Λ baryons that decay early enough for the proton and pion to be reconstructed in the vertex detector; and Λ baryons that decay later, such that they cannot be reconstructed in the vertex detector. These categories are referred to as long and downstream, respectively. The Λ candidates in the long category have a better mass, momentum and vertex resolution than those in the downstream category. Approximately two thirds of the candidates are reconstructed in the downstream category. For both categories, the proton and pion are required to be significantly displaced from all PVs in the event and form a common vertex with a good vertex-fit quality. The Λ candidates are also required to have an invariant mass within $30\,\mathrm{MeV}/c^2$ of the known Λ-baryon mass [53], a decay time larger than 2 ps and a decay vertex at $z < 2350\,\mathrm{mm}$. The z-axis is aligned with the LHC beam line, with positive z in the direction of the LHCb detector acceptance, where $z = 0$ corresponds approximately to the centre of the pp interaction region. The vertex position requirement is imposed to remove background from material interactions in front of the large-area silicon-strip detector. The Λ_b^0 candidate is associated with the PV relative to which it has smallest χ^2_{IP}, where χ^2_{IP} is defined as the difference in the vertex-fit χ^2 of a given PV reconstructed with and without a considered particle. The Λ_b^0 candidate is required to have a good vertex-fit quality, to be consistent with originating from its associated PV and to have a vertex position that is significantly displaced from that PV. A kinematic fit is then performed, constraining the masses of the J/ψ and Λ candidates to their known values [53] and constraining the Λ_b^0 candidate to originate from its associated PV.

The signal candidates are required to have passed a hardware trigger that selects either a single muon with a large transverse momentum or a pair of muons with a large product of their individual transverse momenta. The software trigger requires a candidate to be at least partially reconstructed with a secondary vertex that has a significant displacement from any PV. At least one charged particle must have a large p_{T} and be inconsistent with originating from a PV. A multivariate discriminator [54] is used for the identification of secondary vertices consistent with the decay of a b hadron.

A neural network [55, 56] is trained to reject background from events where tracks have been mistakenly combined to form a signal candidate (combinatorial background). The network is trained using simulated $\Lambda_b^0 \to J/\psi\,\Lambda$ decays as a signal sample and candidates from the data with a $J/\psi\,\Lambda$ invariant mass, $m(J/\psi\,\Lambda)$, larger than $5900\,\mathrm{MeV}/c^2$ as a background sample. The neural network uses the following inputs: the Λ_b^0 decay time and p_{T}; the Λ mass, decay time and p_{T}; the χ^2 of the fitted Λ_b^0 decay vertex; the angle between the Λ_b^0 momentum direction and the vector connecting the primary and Λ_b^0 decay

Table 2: Signal yields in the long and downstream categories of the 2011, 2012, 2015 and 2016 data sets.

	2011	2012	2015	2016
Long	$1\,792 \pm 46$	$4\,099 \pm 74$	925 ± 34	$6\,291 \pm 88$
Downstream	$3\,030 \pm 59$	$7\,904 \pm 96$	$1\,722 \pm 47$	$12\,809 \pm 125$

vertices; and the $\chi^2_{\rm IP}$ of the final-state hadron and muon with the largest $p_{\rm T}$ with respect to its associated PV. Separate classifiers are trained for data taken at different collision energies. A single neural network is used for both long and downstream candidates, with the Λ category used as an input to the network. The working point of the neural network is chosen to maximise $\varepsilon_S S/\sqrt{\varepsilon_S S + \varepsilon_B B}$. Here, S and B are the number of signal and background decays within $14\,{\rm MeV}/c^2$ of the known Λ_b^0 mass [53] (about twice the resolution on the invariant mass) before the application of the classifier, ε_S and ε_B are the efficiencies of the classifier requirement evaluated on the signal and background training samples.

The Λ_b^0 candidates are required to be in the fiducial region, $1 < p_{\rm T} < 20\,{\rm GeV}/c$ and $2 < \eta < 5$. The mean of the $x_{\rm F}$ distribution of the selected Λ_b^0 signal decays varies between 0.015 at $\sqrt{s} = 13\,{\rm TeV}$ and 0.028 at 7 TeV. The corresponding standard deviations of these distributions are 0.008 and 0.014.

Several sources of specific background have been considered. The largest specific background originates from $B^0 \to J/\psi\, K_{\rm S}^0$ decays, where one of the pions from the $K_{\rm S}^0 \to \pi^+\pi^-$ decay is reconstructed as a proton. Background from partially reconstructed b-baryon decays such as $\Lambda_b^0 \to J/\psi\, \Lambda(1520)$, $\Lambda_b^0 \to J/\psi\, \Sigma^0$ or $\Xi_b \to J/\psi\, \Xi$ decays, where the $\Lambda(1520)$, Σ^0 and Ξ subsequently decay to a Λ baryon, give a negligible contribution to the selected sample.

5 Signal yields

The yield of $\Lambda_b^0 \to J/\psi\, \Lambda$ decays in each data set and in each Λ category is determined by performing an extended unbinned maximum-likelihood fit to the $J/\psi\, \Lambda$ mass distribution. The signal is parameterised by the sum of two Crystal Ball (CB) functions [57] combined with a Gaussian function. The two CB functions have a common peak position and width; one has a power-law tail on the lower side of the peak, the other on the upper side of the peak. The Gaussian function shares the same peak position as the two CB functions. The tail parameters and the relative fractions of the three signal components are fixed, for each data set, from fits to simulated $\Lambda_b^0 \to J/\psi\, \Lambda$ decays. The combinatorial background is described by an exponential function. The background from $B^0 \to J/\psi\, K_{\rm S}^0$ decays is described by a CB function with parameters fixed from simulated decays. Figure 2 shows the $m(J/\psi\, \Lambda)$ distribution and the result of the fits for each of the four data-taking years, with the two Λ categories combined. The signal yields in the long and downstream categories of the 2011, 2012, 2015 and 2016 data are given in Table 2.

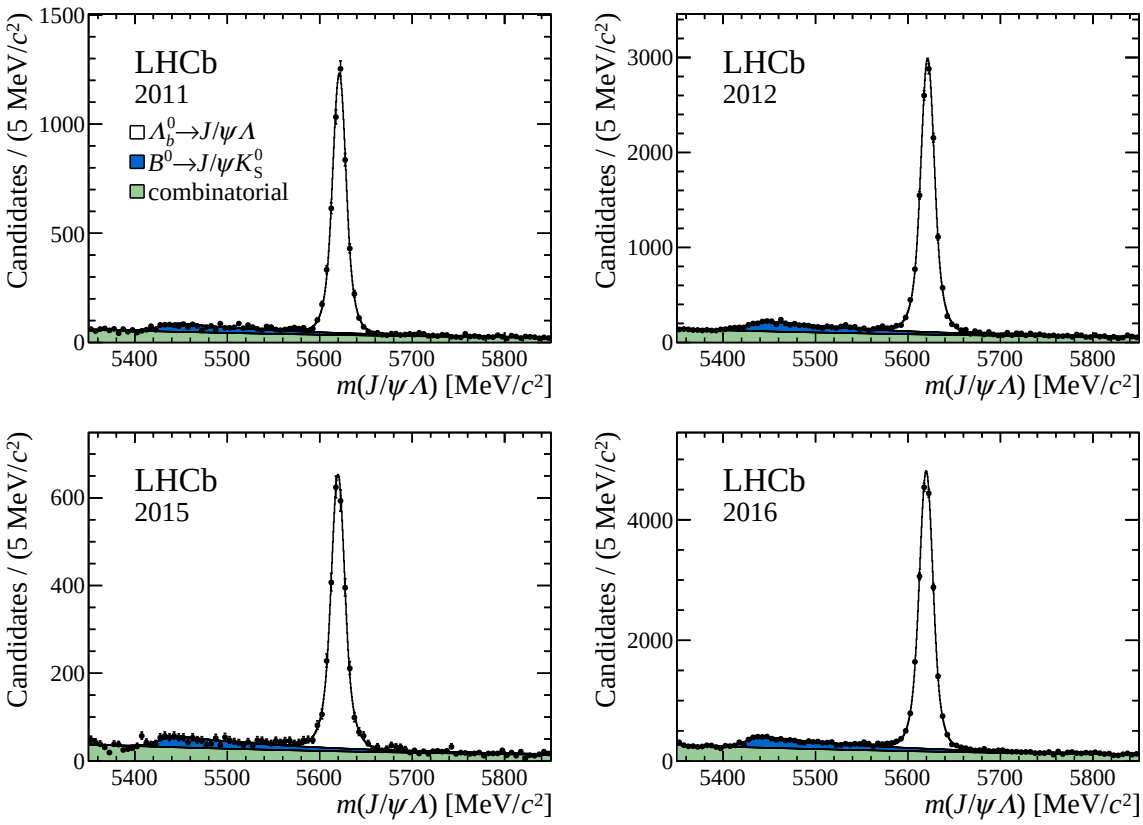

Figure 2: Mass distribution of selected $\Lambda_b^0 \to J/\psi \Lambda$ candidates in (top-left) the 2011, (top-right) the 2012, (bottom-left) the 2015 and (bottom-right) the 2016 data sets. The long and downstream categories have been combined. The results of fits to the distributions are overlaid.

6 Angular efficiency

Both the detector acceptance and candidate selection affect the observed angular distribution of the candidates. As described in Ref. [58], the largest distortions of the angular distribution arise from kinematic requirements in the reconstruction and in the trigger. Corrections for the nonuniformity of the angular efficiency are determined using samples of simulated $\Lambda_b^0 \to J/\psi \Lambda$ decays. The simulated samples are generated with isotropic decays of the Λ_b^0 baryon, the Λ baryon and the J/ψ meson. The resulting angular distribution is uniform in each of the five decay angles. After the selection procedure is applied, the angular distribution of the simulated decays is proportional to the full reconstruction and selection efficiency. A full five-dimensional description is used to parameterise the angular distribution. The parameterisation exploits the orthogonality of Legendre polynomials, $L_j(x)$, and of cosine functions. In its most general form, the distribution and hence the efficiency can be described by the sum

$$\varepsilon(\vec{\Omega}) = \sum_{rstuv} c_{rstuv} L_r(\cos\theta) L_s(\cos\theta_l) L_t(\cos\theta_b) L_u(\phi_b/\pi) \cos(v\phi_l) \ . \tag{3}$$

The coefficients c_{rstuv} are determined by performing a moment analysis of the simulated sample.

To describe the efficiency shape accurately, a large number of terms is needed in each dimension. An absolute normalisation of the efficiency is not needed in this analysis. To

reduce the complexity of the parameterisation, an iterative approach is used, where the efficiency model is constructed in stages. At the first stage, each dimension is parameterised independently and the simulated decays are corrected by the inverse of this simplified efficiency model. At the second stage, three-dimensional corrections are determined separately for ($\cos\theta_l$, ϕ_l, $\cos\theta$) and for ($\cos\theta_b$, ϕ_b, $\cos\theta$), which are subsequently applied to the simulated decays. Finally, a five-dimensional correction is applied according to Eq. 3 with r, s, t, u and v between zero and two. Since the μ^+ and μ^- from the J/ψ have almost identical interactions in the detector, the parameterisation is required to be symmetric in $\cos\theta_l$ and ϕ_l about zero such that only terms with even values of s and v are used in the efficiency model. This assumption is validated on simulated $\Lambda_b^0 \to J/\psi\,\Lambda$ decays, generated with a more realistic decay model. A separate efficiency correction is derived for the long and downstream Λ categories in each data-taking year.

7 Angular moments

The values of the angular terms normalised to the total rate, $M_i = J_i/(2J_1 + J_2)$, can be determined from the data by a moment analysis,

$$M_i = \frac{1}{2J_1 + J_2} \int_{\Omega} \frac{\mathrm{d}^5\Gamma}{\mathrm{d}\vec{\Omega}} g_i(\vec{\Omega}) \mathrm{d}\vec{\Omega} \ , \tag{4}$$

through an appropriate choice of the functions $g_i(\vec{\Omega})$ [37]. The integral can be estimated by a sum over the observed candidates, c,

$$M_i = \left(\sum_{c=1}^{N} w_c g_i(\vec{\Omega}_c) \right) \Big/ \left(\sum_{c=1}^{N} w_c \right) \ , \tag{5}$$

where the weights, w_c, are used to account for both background contamination and the non-uniform angular efficiency of the detector acceptance and the candidate selection and N is the number of observed candidates. The background contamination is subtracted using the *sPlot* technique [59] with $m(J/\psi\,\Lambda)$ as a discriminating variable.

The analysis procedure is validated on $B^0 \to J/\psi\,K_S^0$ decays, where the K_S^0 meson subsequently decays to $\pi^+\pi^-$. This decay has a similar topology to that of the $\Lambda_b^0 \to J/\psi\,\Lambda$ decay but has an angular dependence that is uniform in $\cos\theta$, $\cos\theta_b$, ϕ_l and ϕ_b and depends only on $\sin^2\theta_l$, resulting in $M_1 = \frac{1}{2}$ and the remaining moments being zero. The $B^0 \to J/\psi\,K_S^0$ candidates are selected in data in an analogous way to the $\Lambda_b^0 \to J/\psi\,\Lambda$ candidates. The measured moments for the $B^0 \to J/\psi\,K_S^0$ decay are consistent with expectation and a χ^2 comparison of the moments with their expected values yields a p-value of 12%.

The values of the moments for the $\Lambda_b^0 \to J/\psi\,\Lambda$ decay at the three different centre-of-mass energies are given in Table 3. The results from the long and downstream categories are compatible and are combined in the table. Systematic uncertainties on the moments are discussed in Section 8. The values of moments M_{11} to M_{34} are consistent with zero, indicating a small production polarisation. The statistical covariance matrices for the moments are determined by bootstrapping the data set (*cf.* Ref. [60]) and repeating the analysis procedure. The correlation matrices for the moments are provided in Appendix A.

Figure 3 shows the background-subtracted angular projections of the five decay angles for the selected candidates. Good agreement is seen between the data and the result of the moment analysis. The values of the moments are also found to be in good agreement between Λ_b^0 and $\overline{\Lambda}_b^0$ baryons, indicating that there is no significant difference in the production polarisation or decays of the Λ_b^0 and $\overline{\Lambda}_b^0$ baryons. The numerical values of all moments and the corresponding covariance matrices are available as supplementary material to this article.

Table 3: Values of the 20 moments, M_i, measured in the data collected at 7, 8 and 13 TeV centre-of-mass energies. The long and downstream categories have been combined. The first and second uncertainties are statistical and systematic, respectively.

	7 TeV	8 TeV	13 TeV
M_1	$0.374 \pm 0.007 \pm 0.003$	$0.373 \pm 0.004 \pm 0.002$	$0.380 \pm 0.003 \pm 0.001$
M_2	$0.253 \pm 0.014 \pm 0.005$	$0.254 \pm 0.008 \pm 0.003$	$0.239 \pm 0.006 \pm 0.002$
M_4	$-0.286 \pm 0.017 \pm 0.008$	$-0.268 \pm 0.011 \pm 0.009$	$-0.273 \pm 0.008 \pm 0.006$
M_5	$-0.157 \pm 0.025 \pm 0.008$	$-0.181 \pm 0.015 \pm 0.007$	$-0.179 \pm 0.011 \pm 0.005$
M_7	$0.051 \pm 0.029 \pm 0.005$	$0.025 \pm 0.018 \pm 0.003$	$0.022 \pm 0.013 \pm 0.002$
M_9	$-0.017 \pm 0.029 \pm 0.005$	$-0.011 \pm 0.018 \pm 0.003$	$-0.027 \pm 0.013 \pm 0.002$
M_{11}	$0.005 \pm 0.014 \pm 0.004$	$0.003 \pm 0.009 \pm 0.004$	$-0.005 \pm 0.006 \pm 0.002$
M_{12}	$-0.004 \pm 0.018 \pm 0.005$	$0.010 \pm 0.011 \pm 0.004$	$0.006 \pm 0.008 \pm 0.003$
M_{14}	$0.007 \pm 0.025 \pm 0.007$	$-0.015 \pm 0.016 \pm 0.007$	$-0.009 \pm 0.012 \pm 0.003$
M_{15}	$-0.027 \pm 0.032 \pm 0.008$	$0.009 \pm 0.021 \pm 0.008$	$-0.006 \pm 0.016 \pm 0.005$
M_{17}	$0.008 \pm 0.039 \pm 0.006$	$-0.002 \pm 0.025 \pm 0.004$	$0.011 \pm 0.018 \pm 0.003$
M_{19}	$-0.006 \pm 0.038 \pm 0.004$	$-0.015 \pm 0.025 \pm 0.004$	$-0.003 \pm 0.018 \pm 0.002$
M_{21}	$-0.015 \pm 0.037 \pm 0.008$	$0.007 \pm 0.022 \pm 0.005$	$-0.032 \pm 0.016 \pm 0.005$
M_{23}	$-0.001 \pm 0.028 \pm 0.007$	$-0.022 \pm 0.017 \pm 0.003$	$0.018 \pm 0.012 \pm 0.002$
M_{25}	$-0.029 \pm 0.064 \pm 0.010$	$-0.001 \pm 0.038 \pm 0.008$	$0.044 \pm 0.029 \pm 0.006$
M_{27}	$0.059 \pm 0.051 \pm 0.007$	$0.014 \pm 0.030 \pm 0.005$	$0.038 \pm 0.023 \pm 0.006$
M_{30}	$-0.000 \pm 0.023 \pm 0.004$	$-0.028 \pm 0.014 \pm 0.005$	$0.008 \pm 0.010 \pm 0.003$
M_{32}	$-0.001 \pm 0.021 \pm 0.005$	$0.013 \pm 0.014 \pm 0.004$	$-0.022 \pm 0.010 \pm 0.003$
M_{33}	$0.019 \pm 0.021 \pm 0.005$	$-0.017 \pm 0.013 \pm 0.003$	$-0.007 \pm 0.009 \pm 0.002$
M_{34}	$0.017 \pm 0.021 \pm 0.004$	$0.033 \pm 0.013 \pm 0.004$	$0.008 \pm 0.009 \pm 0.002$

8 Systematic uncertainties

Sources of systematic uncertainty are considered if they either impact the fit to the $m(J/\psi\,\Lambda)$ distribution, and the subsequent background subtraction, or would directly bias the measured angular distribution. The various sources of systematic uncertainty on this measurement are discussed below and summarised in Table 4.

A systematic uncertainty is assigned to cover the knowledge of the signal lineshape parameters by repeating the analysis 1000 times, varying the lineshape parameters within their uncertainties. The resulting systematic uncertainty is given by the standard deviation of the moments evaluated with the different variations.

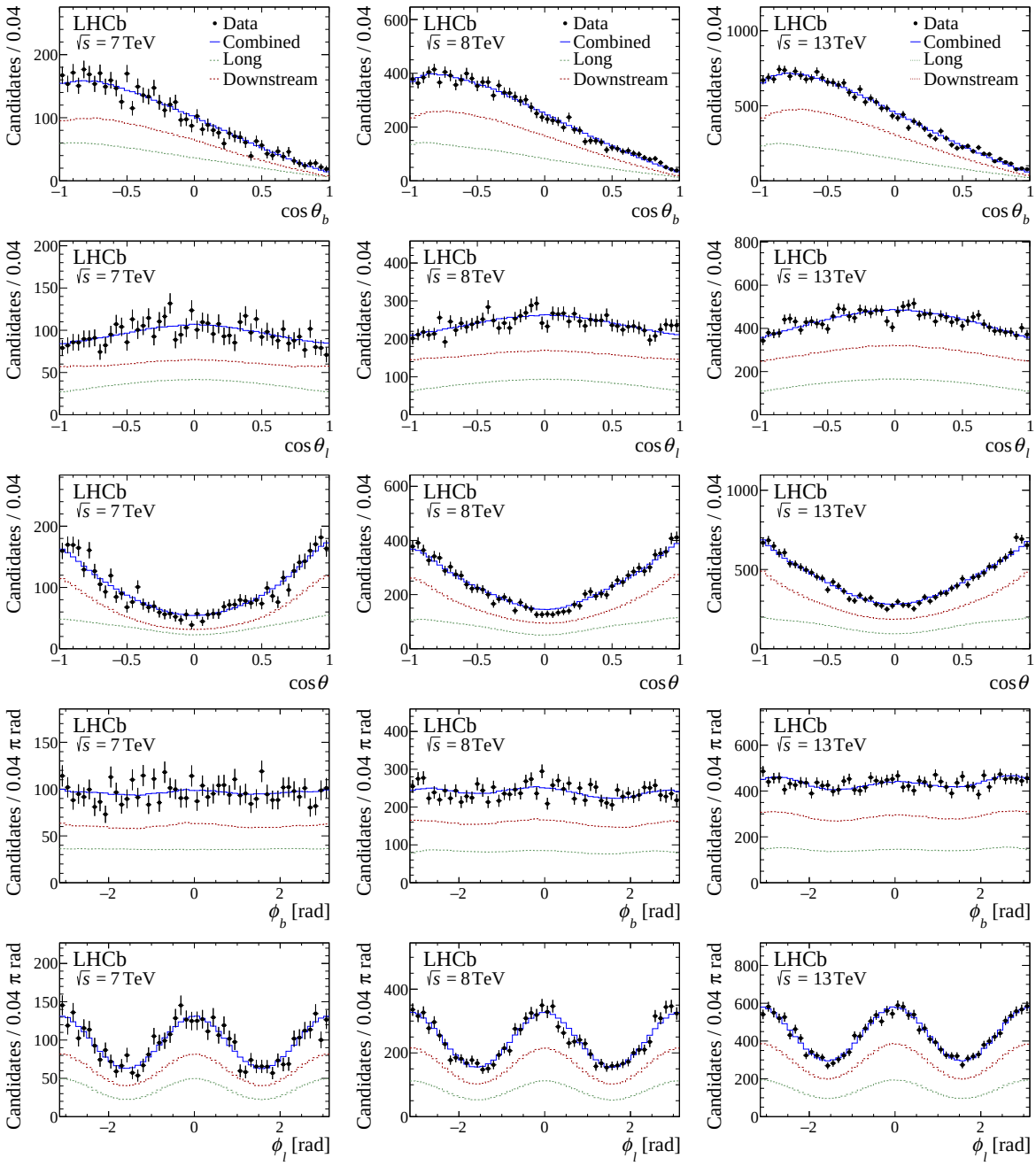

Figure 3: Angular distributions of $\cos\theta_b$, $\cos\theta_l$, $\cos\theta$, ϕ_b and ϕ_l for the background-subtracted candidates. The long and downstream categories for the different data-taking years have been combined. The result of the moment analysis, folded with the angular efficiency, is overlaid. The contribution from the long and downstream categories are indicated by the green and red lines, respectively.

The impact of statistical uncertainty on the efficiency model, due to the limited size of the simulated samples, is determined by bootstrapping the simulated samples 1000 times and rederiving the efficiency models. For each bootstrap, a new set of efficiency coefficients, c_{rstuv}, is determined and the angular moments are reevaluated. For each moment, the standard deviation of the distribution of the difference between the new and the nominal values is assigned as a systematic uncertainty.

To evaluate the impact of the limited number of terms used for the efficiency model, a new parameterisation is determined that allows for higher-order terms in each dimension. Pseudoexperiments are then generated from the higher-order model and the values of the moments determined from each pseudoexperiment using the nominal model. The average bias on the determined value of the moments and its uncertainty are added in quadrature and are assigned as a systematic uncertainty.

A systematic uncertainty is assigned to cover the choice of criteria used to match reconstructed and true particles in the simulation. This uncertainty is evaluated using pseudoexperiments that are generated from an efficiency model derived with a less strict set of matching requirements. The moments are then evaluated with the nominal model. As before, the average bias on the determined value of the moments and its uncertainty are added in quadrature and are assigned as a systematic uncertainty.

The impact of neglecting the detector's angular resolution in the analysis is explored using pseudoexperiments in which the simulated angles are smeared according to the resolution. The resolution, determined using simulated decays, is approximately 3 mrad in θ and θ_l, 20 mrad in θ_b, 10 mrad in ϕ_l and 45 mrad in ϕ_b. The resolution of the long and downstream categories are similar after constraining the masses of the J/ψ and Λ candidates to their known values. The angular moments are then determined from the pseudoexperiments, neglecting the resolution. The average bias on the determined value of the moments and its uncertainty are added in quadrature and are assigned as a systematic uncertainty. The analysis procedure also assumes that the mass and angular variables factorise for both the signal and the background. No significant correlation is found between the mass and angular distribution of simulated $\Lambda_b^0 \to J/\psi\,\Lambda$ decays. The variables are also found to be uncorrelated for the combinatorial background. However, a correlation is seen between the mass and angular distributions of misidentified $B^0 \to J/\psi\,K_S^0$ decays. The impact of neglecting this correlation is tested using pseudoexperiments, with the mass and angular distributions of the $B^0 \to J/\psi\,K_S^0$ decays taken from a detailed simulation. The values of the moments are then determined neglecting the correlation and the resulting bias is taken as a systematic uncertainty. In principle there is also an effect arising from neglecting the precession of the Λ-baryon spin in the external magnetic field of the experiment. The precession is small due to the small size of the integrated field between the production and decay points of the Λ baryon.

The track-reconstruction and muon-identification efficiency of the LHCb detector are determined from data, in bins of p_T and η, using a tag-and-probe approach with $J/\psi \to \mu^+\mu^-$ decays [40]. The resulting corrections to the simulation are small and are neglected in the analysis. The impact of neglecting these corrections is evaluated using pseudoexperiments. The pseudoexperiments are generated from an efficiency model that takes into account the corrections. The moments are then determined using a model that neglects the corrections and a systematic uncertainty is assigned based on the average bias on the moments and its uncertainty.

The trigger efficiency of the hardware trigger is also determined in data, as a function

Table 4: Systematic uncertainties on the angular moments. The largest value amongst the moments is given for each source. The total systematic uncertainty varies from 0.002 to 0.010, depending on the moment considered. The sources are described in the text.

Source	Uncertainty
Mass model	0.003
Simulation sample size	0.006
Polynomial order	0.004
Truth matching criteria	0.007
Angular resolution	0.003
Factorisation of mass and angles	0.003
Tracking and muon-identification efficiency	0.005
Trigger efficiency modelling	0.003
Kinematic weighting	0.006
Beam-crossing angle	0.001

of the muon p_{T}, using the method described in Ref. [45]. The impact of the resulting corrections to the simulation is again investigated with pseudoexperiments. The pseudoexperiments are generated taking into account corrections to the trigger efficiency and the moments are determined neglecting the corrections. The resulting uncertainty is assigned based on the average bias and its uncertainty.

A systematic uncertainty is assigned to the kinematic weighting of the simulated samples using pseudoexperiments. The pseudoexperiments are generated using the nominal model from which moments are determined using an efficiency model that neglects the kinematic corrections. Again, the average bias and its uncertainty are added in quadrature and are assigned as the systematic uncertainty.

Finally, a systematic uncertainty is evaluated to cover the uncertainty on the beam crossing angle at the LHCb interaction point. This is estimated using simulated events in which the crossing angle is varied. The resulting systematic uncertainty is negligible.

The total systematic uncertainty on each moment is determined by summing the individual sources of uncertainty in quadrature. The resulting values are given in Table 3. The systematic uncertainty is typically less than half the size of the statistical uncertainty on a given moment. Correlated systematic uncertainties between different moments are found to be small as are correlations between the different data sets. Correlations between systematic uncertainties are therefore neglected when determining the decay amplitudes and production polarisation.

9 Decay amplitudes and production polarisation

The decay amplitudes and the production polarisation are determined from the moments using a Bayesian analysis. The marginalisation over unwanted parameters is performed using Markov Chain Monte Carlo, with the Metropolis-Hastings algorithm employed to sample points in the parameter space [61, 62]. The likelihood at each point in the

Table 5: Estimates for the magnitude and phase of the decay amplitudes and the transverse production polarisation of the Λ_b^0 baryons, extracted using the Bayesian analysis. The most probable value (MPV) and the shortest 68% interval containing the most probable value are given.

Observable	MPV	Interval
$\lvert a_+\rvert$	0.129	[0.033, 0.163]
$\lvert a_-\rvert$	1.021	[0.998, 1.041]
$\lvert b_-\rvert$	0.145	[0.060, 0.188]
$\arg(a_+)$ [rad]	-2.523	$[-\pi, -1.131]$ or $[2.117, \pi]$
$\arg(a_-)$ [rad]	1.122	$[-2.633, -1.759]$ or $[0.101, 2.224]$
$\arg(b_-)$ [rad]	1.788	$[-\pi, -2.275]$ or $[0.232, \pi]$
P_b (7 TeV)	-0.004	$[-0.064, 0.051]$
P_b (8 TeV)	0.001	$[-0.035, 0.045]$
P_b (13 TeV)	0.032	$[-0.011, 0.065]$
α_b	-0.022	$[-0.048, 0.005]$

parameter space is given by

$$L = \left[\prod_{\text{data set } j} \exp(-\tfrac{1}{2}\vec{D}_j^{\mathrm{T}} C_j^{-1} \vec{D}_j) \right] \times \exp\left(-\frac{1}{2} \left(\frac{\alpha_\Lambda - \alpha_\Lambda^{\mathrm{BES}}}{\sigma(\alpha_\Lambda^{\mathrm{BES}})} \right)^2 \right) , \tag{6}$$

where $\vec{D}_j$ is a vector representing the difference between the measured values of the moments and the values of the moments at that point in the parameter space and C_j is the covariance matrix combining the statistical and systematic uncertainties on the moments. The last term in the likelihood originates from the external constraints from BESIII on the value of α_Λ. In this analysis, the recent BESIII result [34] for the Λ asymmetry parameter is used. Averaging the BESIII values for Λ and $\overline{\Lambda}$ decays yields $\alpha_\Lambda^{\mathrm{BES}} = 0.754$ with an uncertainty $\sigma(\alpha_\Lambda^{\mathrm{BES}}) = 0.003$. The value of α_Λ and the values of the complex amplitudes $a_\pm$ and $b_\pm$ are shared between the different data sets but the polarisation is allowed to differ between different centre-of-mass energies. The Bayesian analysis procedure has been validated for both small and large values of the polarisation using pseudoexperiments.

The resulting marginal posterior distributions for the amplitudes and polarisation are shown in Figure 4. The magnitude and phase of b_+ are fixed to be $|b_+| = 1$ and $\arg(b_+) = 0$. This amplitude is one of the two amplitudes that are expected to be large. The remaining amplitudes are measured relative to b_+. A uniform prior is assumed on their magnitudes and phases and on P_b. The priors use the ranges $[-1, +1]$ for P_b, $[-\pi, +\pi]$ for the phases, and the range $[0, 20]$ for the magnitudes of the amplitudes. The values of the amplitudes and the polarisations are given in Table 5. The 95% credibility intervals are provided in Table 6 of the Appendix. Figure 5 shows P_b as a function of the $\sqrt{s}$ of the data set. The resulting Λ_b^0 polarisation at each centre-of-mass energy is found to be consistent with zero.

The Markov chain finds two almost-degenerate solutions, which correspond to a change in sign of the polarisation accompanied by a change in sign of the decay amplitudes. This occurs due to the small size of two of the amplitudes. The degeneracy is most visible in

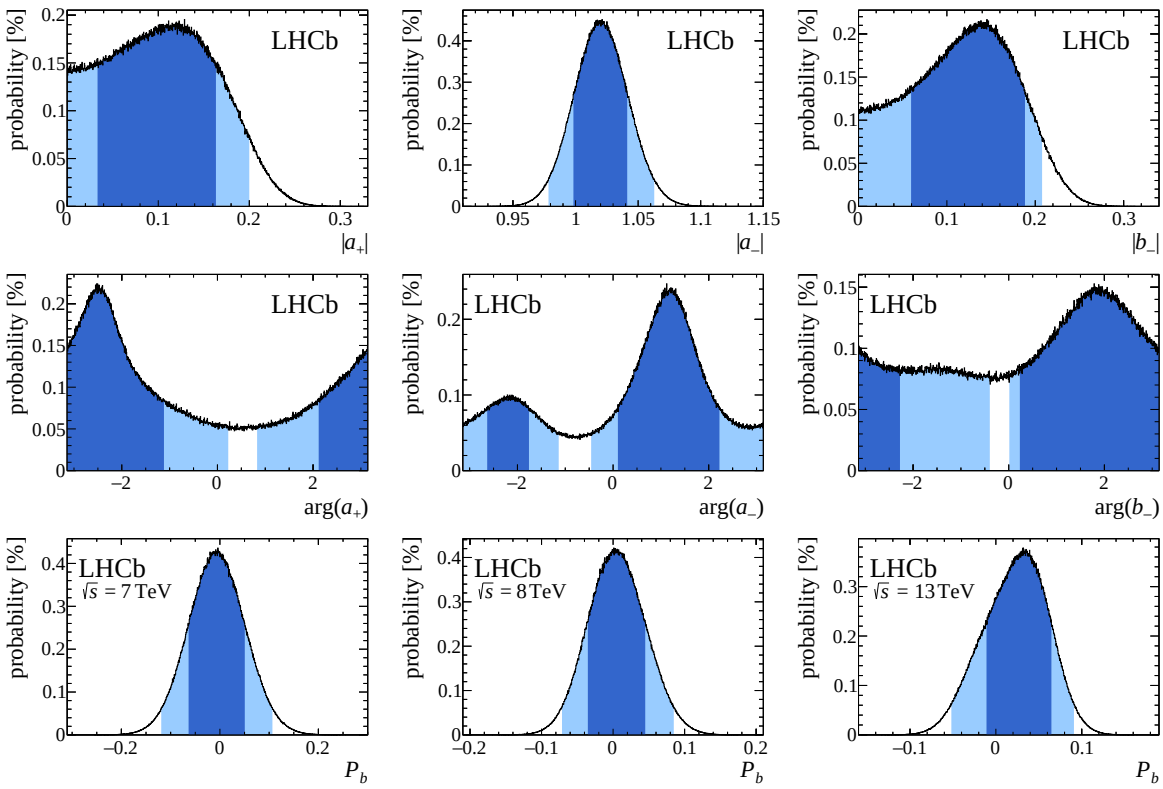

Figure 4: Posterior probability distributions of $|a_\pm|$, $\arg(a_\pm)$, $|b_-|$, $\arg(b_-)$ and the transverse production polarisation of the Λ_b^0 baryons, P_b, at centre-of-mass energies of 7, 8 and 13 TeV assuming uniform priors. The shaded regions indicate the 68% and 95% credibility intervals.

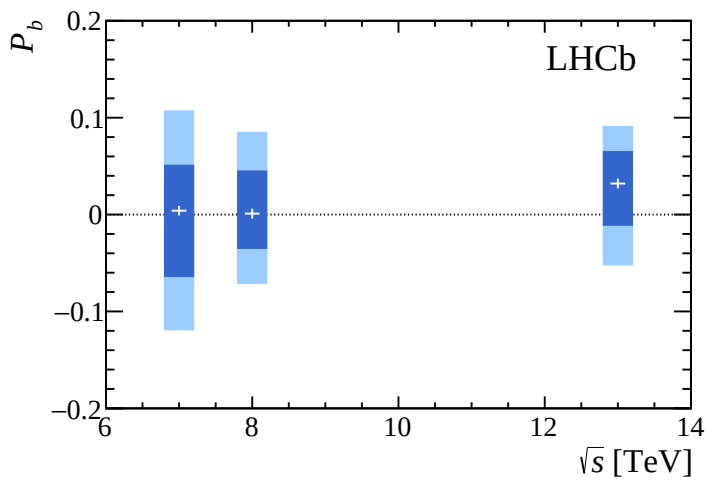

Figure 5: Measured transverse production polarisation of the Λ_b^0 baryons, P_b, as a function of the centre-of-mass energy, $\sqrt{s}$, of the data set. The points indicate the most probable value and the shaded regions the 68% and 95% credibility level intervals.

the posterior distribution of P_b determined at $\sqrt{s}$ of 13 TeV, leading to an asymmetric distribution. Due to the small size of polarisation, there is little sensitivity to the phases of the amplitudes. The magnitudes of the amplitudes a_+ and b_- are consistent with zero

at the 95% credibility level, as expected in the heavy-quark limit. The magnitudes of a_- and b_+ are found to be similar in size. Figure 6 shows the posterior distribution of the parity-violating asymmetry parameter, α_b, from the Bayesian analysis. The most probable value of α_b is -0.022. The 68% credibility interval around the most probable value is $[-0.048, 0.005]$. This measurement is consistent with, but more precise than, previous measurements of α_b by the ATLAS, CMS and LHCb collaborations [26–28].

The posterior distribution of α_Λ with the constraint on α_Λ removed, assuming a uniform prior in the range $[-1, +1]$, is shown in Fig. 7. The most probable value of α_Λ is 0.74. The 68% credibility interval spans $[0.71, 0.78]$. The data strongly favour the larger α_Λ value reported by the BESIII collaboration [34] over the values from older secondary scattering measurements [29–33], which are excluded with high significance. Small values of α_Λ are excluded by the large $p\pi^-$ forward-backward asymmetry observed in the $\cos\theta_b$ distribution. Larger values of α_Λ can be accommodated by changing the magnitudes of the decay amplitudes to reduce the asymmetry.

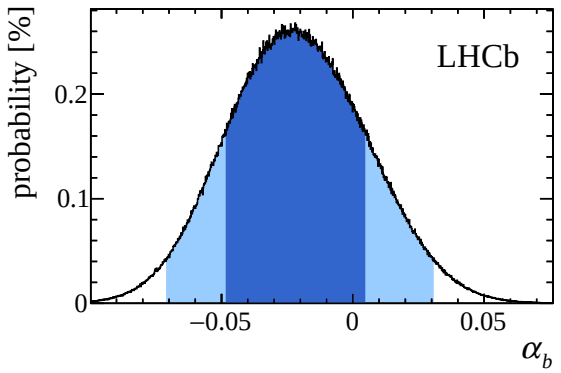

Figure 6: Posterior probability distribution of the parity-violating asymmetry parameter, α_b. The shaded regions indicate the 68% and 95% credibility intervals.

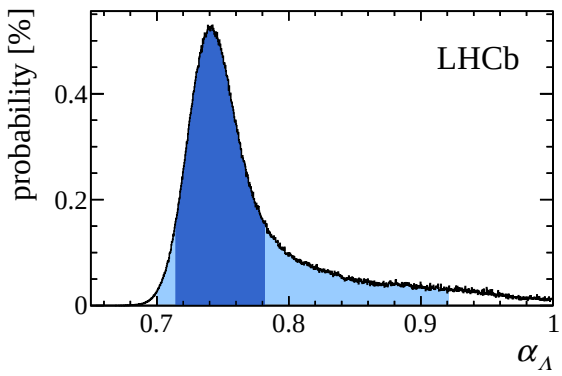

Figure 7: Posterior probability distribution for α_Λ, assuming a uniform prior, with all external constraints removed. The shaded regions indicate the 68% and 95% credibility intervals.

10 Summary

This paper presents a measurement of the decay amplitudes parameterising the $\Lambda_b^0 \to J/\psi\,\Lambda$ angular distribution, and a measurement of the transverse production polarisation of the Λ_b^0 baryons at $\sqrt{s}$ of 7, 8 and 13 TeV, using data collected with the LHCb experiment. The measurements are performed in a fiducial region of Λ_b^0 transverse momentum and pseudorapidity of $1 < p_{\mathrm{T}} < 20\,\mathrm{GeV}/c$ and $2 < \eta < 5$, respectively. The magnitudes of two of the four decay amplitudes are found to be small. One of these amplitudes corresponds to Λ helicity of $+\frac{1}{2}$ and J/ψ helicity of 0 and the other to Λ helicity of $-\frac{1}{2}$ and J/ψ helicity of -1. This is consistent with the expectation from the heavy-quark limit and the left-handed nature of the weak interaction. The parity-violating parameter α_b is found to be consistent with zero, with a 68% credibility interval from -0.048 to 0.005. The small negative value of α_b favoured by the data is consistent with most theoretical predictions but is inconsistent with the prediction based on HQET in Ref. [5]. The Λ_b^0 production polarisation is found to be consistent with zero, with 68% credibility level intervals of $[-0.06, 0.05]$, $[-0.04, 0.05]$ and $[-0.01, 0.07]$ at $\sqrt{s}$ of 7, 8 and 13 TeV, respectively. The results in this paper supersede those of Ref. [26] and are largely consistent with the previous measurements [26–28]. Differences between the results presented in this paper and the previous measurements can be attributed to the value of α_Λ used in those measurements. The data strongly support the recent BESIII measurement of α_Λ over the previous value from secondary scattering data. With the old value of α_Λ, it is not possible to describe the data with a physical set of amplitudes.

Acknowledgements

We express our gratitude to our colleagues in the CERN accelerator departments for the excellent performance of the LHC. We thank the technical and administrative staff at the LHCb institutes. We acknowledge support from CERN and from the national agencies: CAPES, CNPq, FAPERJ and FINEP (Brazil); MOST and NSFC (China); CNRS/IN2P3 (France); BMBF, DFG and MPG (Germany); INFN (Italy); NWO (Netherlands); MNiSW and NCN (Poland); MEN/IFA (Romania); MSHE (Russia); MinECo (Spain); SNSF and SER (Switzerland); NASU (Ukraine); STFC (United Kingdom); DOE NP and NSF (USA). We acknowledge the computing resources that are provided by CERN, IN2P3 (France), KIT and DESY (Germany), INFN (Italy), SURF (Netherlands), PIC (Spain), GridPP (United Kingdom), RRCKI and Yandex LLC (Russia), CSCS (Switzerland), IFIN-HH (Romania), CBPF (Brazil), PL-GRID (Poland) and OSC (USA). We are indebted to the communities behind the multiple open-source software packages on which we depend. Individual groups or members have received support from AvH Foundation (Germany); EPLANET, Marie Skłodowska-Curie Actions and ERC (European Union); ANR, Labex P2IO and OCEVU, and Région Auvergne-Rhône-Alpes (France); Key Research Program of Frontier Sciences of CAS, CAS PIFI, and the Thousand Talents Program (China); RFBR, RSF and Yandex LLC (Russia); GVA, XuntaGal and GENCAT (Spain); the Royal Society and the Leverhulme Trust (United Kingdom).

Appendices

A Correlation matrices

The statistical correlations between the different moments determined at the three different centre-of-mass energies are shown in Figs. 8, 9 and 10. The correlation coefficients are determined by bootstrapping the data set. The covariance matrices are available as supplementary material to this article.

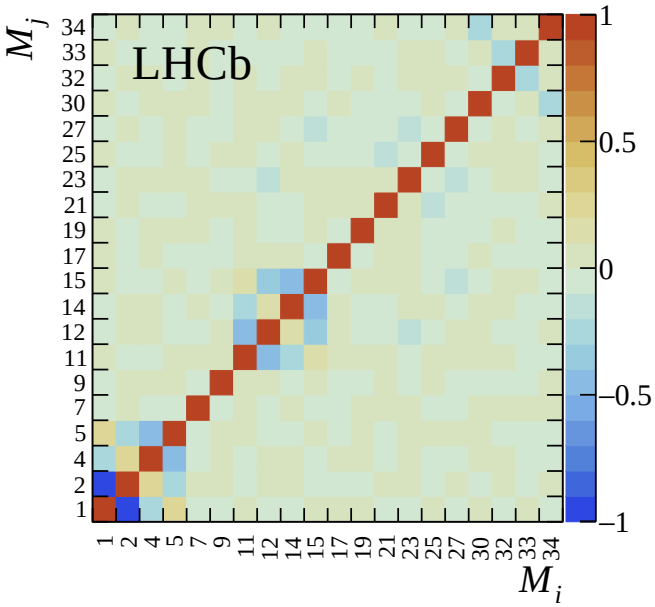

Figure 8: Statistical correlation between the moments determined at $\sqrt{s}$ of 7 TeV.

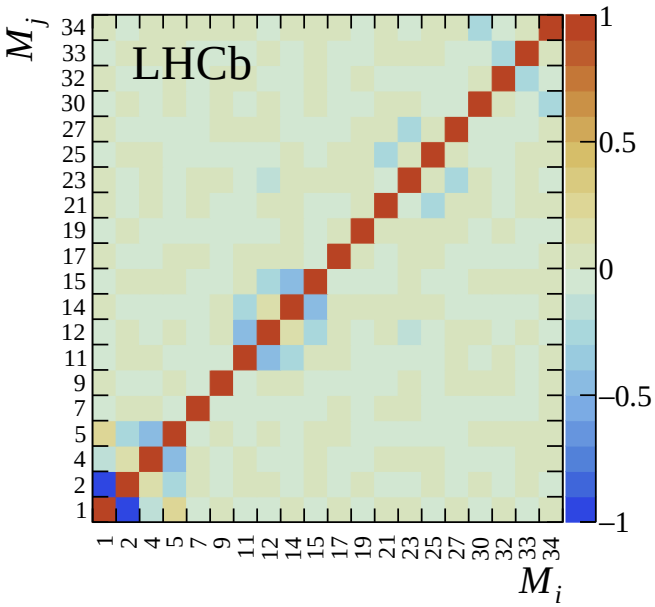

Figure 9: Statistical correlation between the moments determined at $\sqrt{s}$ of 8 TeV.

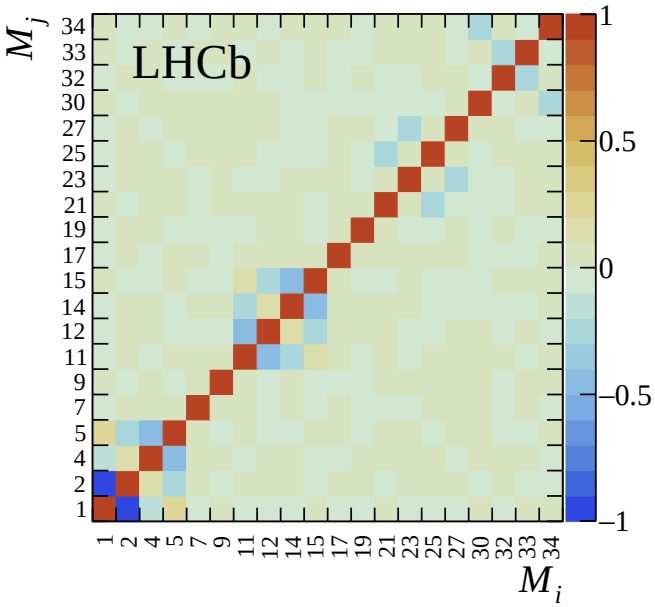

Figure 10: Statistical correlation between the moments determined at $\sqrt{s}$ of 13 TeV.

B Intervals at 95% credibility level

The 95% credibility level intervals on the decay amplitudes and production polarisation from the Bayesian analysis of the moments are given in Table 6. The 95% intervals on α_b and on α_Λ are also provided. The interval on α_Λ is evaluated after removing the external constraint on that parameter.

Table 6: Intervals at 95% credibility level on the amplitudes, the polarisation and α_b from the Bayesian analysis. The interval on α_Λ, with the external constraint removed, is also provided.

Observable	Interval
$\lvert a_+\rvert$	$[\ 0.000,\ \ 0.200]$
$\lvert a_-\rvert$	$[\ 0.978,\ \ 1.063]$
$\lvert b_-\rvert$	$[\ 0.000,\ \ 0.208]$
$\arg(a_+)$ [rad]	$[-\pi,\ \ 0.251]$ or $[\ 0.848, \pi]$
$\arg(a_-)$ [rad]	$[-\pi, -1.137]$ or $[-0.459, \pi]$
$\arg(b_-)$ [rad]	$[-\pi, -0.396]$ or $[\ 0.013, \pi]$
P_b (7 TeV)	$[-0.119,\ \ 0.107]$
P_b (8 TeV)	$[-0.071,\ \ 0.085]$
P_b (13 TeV)	$[-0.052,\ \ 0.091]$
α_b	$[-0.071,\ \ 0.031]$
α_Λ	$[\ 0.700,\ \ 0.921]$

References

[1] G. Hiller, M. Knecht, F. Legger, and T. Schietinger, *Photon polarization from helicity suppression in radiative decays of polarized Λ_b^0 to spin-3/2 baryons*, Phys. Lett. **B649** (2007) 152, `arXiv:hep-ph/0702191`.

[2] T. Mannel and G. A. Schuler, *Semileptonic decays of bottom baryons at LEP*, Phys. Lett. **B279** (1992) 194.

[3] A. F. Falk and M. E. Peskin, *Production, decay, and polarization of excited heavy hadrons*, Phys. Rev. **D49** (1994) 3320, `arXiv:hep-ph/9308241`.

[4] W. G. D. Dharmaratna and G. R. Goldstein, *Single quark polarization in quantum chromodynamics subprocesses*, Phys. Rev. **D53** (1996) 1073.

[5] Z. J. Ajaltouni, E. Conte, and O. Leitner, *Λ_b^0 decays into Λ-vector*, Phys. Lett. **B614** (2005) 165, `arXiv:hep-ph/0412116`.

[6] E. J. Ramberg *et al.*, *Polarization of Λ and $\overline{\Lambda}$ produced by 800-GeV protons*, Phys. Lett. **B338** (1994) 403.

[7] V. Fanti *et al.*, *A Measurement of the transverse polarization of Λ hyperons produced in inelastic pN reactions at 450-GeV proton energy*, Eur. Phys. J. **C6** (1999) 265.

[8] HERA-B collaboration, I. Abt *et al.*, *Polarization of Λ and $\overline{\Lambda}$ in 920-GeV fixed-target proton-nucleus collisions*, Phys. Lett. **B638** (2006) 415, `arXiv:hep-ex/0603047`.

[9] CDF collaboration, T. Aaltonen *et al.*, *First observation of heavy baryons Σ_b and Σ_b^**, Phys. Rev. Lett. **99** (2007) 202001, `arXiv:0706.3868`.

[10] LHCb collaboration, R. Aaij *et al.*, *Observation of excited Λ_b^0 baryons*, Phys. Rev. Lett. **109** (2012) 172003, `arXiv:1205.3452`.

[11] CDF collaboration, T. A. Aaltonen *et al.*, *Evidence for a bottom baryon resonance Λ_b^{*0} in CDF data*, Phys. Rev. **D88** (2013) 071101, `arXiv:1308.1760`.

[12] LHCb collaboration, R. Aaij *et al.*, *Observation of new resonances in the $\Lambda_b^0\pi^+\pi^-$ system*, Phys. Rev. Lett. **123** (2019) 152001, `arXiv:1907.13598`.

[13] CMS collaboration, A. M. Sirunyan *et al.*, *Study of excited Λ_b^0 states decaying to $\Lambda_b^0\pi^+\pi^-$ in proton-proton collisions at $\sqrt{s} = 13$ TeV*, `arXiv:2001.06533`.

[14] T. D. Lee and C.-N. Yang, *General partial wave analysis of the decay of a hyperon of spin 1/2*, Phys. Rev. **108** (1957) 1645.

[15] H.-Y. Cheng, *Nonleptonic weak decays of bottom baryons*, Phys. Rev. **D56** (1997) 2799, Erratum ibid. **D99** (2019) 079901, `arXiv:hep-ph/9612223`.

[16] Fayyazuddin and Riazuddin, *Two-body nonleptonic Λ_b^0 decays in quark model with factorization ansatz*, Phys. Rev. **D58** (1998) 014016, `arXiv:hep-ph/9802326`.

[17] Fayyazuddin and M. J. Aslam, *Hadronic weak decay $\mathcal{B}_b(\frac{1}{2}^+) \to \mathcal{B}(\frac{1}{2}^+,\ \frac{3}{2}^+) + V$*, Phys. Rev. **D95** (2017) 113002, `arXiv:1705.05106`.

[18] R. Mohanta *et al.*, *Hadronic weak decays of Λ_b baryon in the covariant oscillator quark model*, Prog. Theor. Phys. **101** (1999) 959, `arXiv:hep-ph/9904324`.

[19] Z.-T. Wei, H.-W. Ke, and X.-Q. Li, *Evaluating decay rates and asymmetries of Λ_b^0 into light baryons in LFQM*, Phys. Rev. **D80** (2009) 094016, `arXiv:0909.0100`.

[20] C.-H. Chou, H.-H. Shih, S.-C. Lee, and H.-n. Li, *$\Lambda_b^0 \to \Lambda J/\psi$ decay in perturbative QCD*, Phys. Rev. **D65** (2002) 074030, `arXiv:hep-ph/0112145`.

[21] T. Gutsche, M. A. Ivanov, J. G. Körner, and V. E. Lyubovitskij, *Nonleptonic two-body decays of single heavy baryons Λ_Q, Ξ_Q, and Ω_Q ($Q = b, c$) induced by W emission in the covariant confined quark model*, Phys. Rev. **D98** (2018) 074011, `arXiv:1806.11549`.

[22] T. Gutsche *et al.*, *Theoretical description of the decays $\Lambda_b^0 \to \Lambda^{(*)}(\frac{1}{2}^\pm, \frac{3}{2}^\pm) + J/\psi$*, Phys. Rev. **D96** (2017) 013003, `arXiv:1705.07299`.

[23] ALEPH collaboration, D. Buskulic *et al.*, *Measurement of Λ_b^0 polarization in Z decays*, Phys. Lett. **B365** (1996) 437.

[24] OPAL collaboration, G. Abbiendi *et al.*, *Measurement of the average polarization of b baryons in hadronic Z^0 decays*, Phys. Lett. **B444** (1998) 539, `arXiv:hep-ex/9808006`.

[25] DELPHI collaboration, P. Abreu *et al.*, *Λ_b^0 polarization in Z^0 decays at LEP*, Phys. Lett. **B474** (2000) 205.

[26] LHCb collaboration, R. Aaij *et al.*, *Measurements of the $\Lambda_b^0 \to J/\psi\,\Lambda$ decay amplitudes and the Λ_b^0 polarisation in pp collisions at $\sqrt{s} = 7$ TeV*, Phys. Lett. **B724** (2013) 27, `arXiv:1302.5578`.

[27] CMS collaboration, A. M. Sirunyan *et al.*, *Measurement of the Λ_b^0 polarization and angular parameters in $\Lambda_b^0 \to J/\psi\,\Lambda$ decays from pp collisions at $\sqrt{s} = 7$ and 8 TeV*, Phys. Rev. **D97** (2018) 072010, `arXiv:1802.04867`.

[28] ATLAS collaboration, G. Aad *et al.*, *Measurement of the parity-violating asymmetry parameter α_b and the helicity amplitudes for the decay $\Lambda_b^0 \to J/\psi\,\Lambda$ with the ATLAS detector*, Phys. Rev. **D89** (2014) 092009, `arXiv:1404.1071`.

[29] P. Astbury *et al.*, *Measurement of the differential cross-section and the spin-correlation parameters P, A, and R in the backward peak of $\pi^- p \to K_S^0 \Lambda$ at 5 GeV/c*, Nucl. Phys. **B99** (1975) 30.

[30] W. E. Cleland *et al.*, *A measurement of the β-parameter in the charged nonleptonic decay of the Λ hyperon*, Nucl. Phys. **B40** (1972) 221.

[31] P. M. Dauber *et al.*, *Production and decay of cascade hyperons*, Phys. Rev. **179** (1969) 1262.

[32] O. E. Overseth and R. F. Roth, *Time reversal invariance in Λ decay*, Phys. Rev. Lett. **19** (1967) 391.

[33] J. W. Cronin and O. E. Overseth, *Measurement of the decay parameters of the Λ particle*, Phys. Rev. **129** (1963) 1795.

[34] BESIII collaboration, M. Ablikim *et al.*, *Polarization and entanglement in baryon-antibaryon pair production in electron-positron annihilation*, Nature Physics **15** (2019) 631, `arXiv:1808.08917`.

[35] D. G. Ireland *et al.*, *Kaon photoproduction and the Λ decay parameter α_-*, Phys. Rev. Lett. **123** (2019) 182301, `arXiv:1904.07616`.

[36] T. Blake, S. Meinel, and D. van Dyk, *Bayesian analysis of $b \to s\mu^+\mu^-$ Wilson coefficients using the full angular distribution of $\Lambda_b^0 \to \Lambda(\to p\,\pi^-)\mu^+\mu^-$ decays*, Phys. Rev. D (2020) 035023, `arXiv:1912.05811`.

[37] T. Blake and M. Kreps, *Angular distribution of polarised Λ_b baryons decaying to $\Lambda\ell^+\ell^-$*, JHEP **11** (2017) 138, `arXiv:1710.00746`.

[38] J. Hrivnac, R. Lednicky, and M. Smizanska, *Feasibility of beauty baryon polarization measurement in $\Lambda^0 J/\psi$ decay channel by ATLAS LHC*, J. Phys. **G21** (1995) 629, `arXiv:hep-ph/9405231`.

[39] LHCb collaboration, A. A. Alves Jr. *et al.*, *The LHCb detector at the LHC*, JINST **3** (2008) S08005.

[40] LHCb collaboration, R. Aaij *et al.*, *LHCb detector performance*, Int. J. Mod. Phys. **A30** (2015) 1530022, arXiv:1412.6352.

[41] R. Aaij *et al.*, *Performance of the LHCb Vertex Locator*, JINST **9** (2014) P09007, arXiv:1405.7808.

[42] R. Arink *et al.*, *Performance of the LHCb Outer Tracker*, JINST **9** (2014) P01002, arXiv:1311.3893.

[43] P. d'Argent *et al.*, *Improved performance of the LHCb Outer Tracker in LHC Run 2*, JINST **12** (2017) P11016, arXiv:1708.00819.

[44] A. A. Alves Jr. *et al.*, *Performance of the LHCb muon system*, JINST **8** (2013) P02022, arXiv:1211.1346.

[45] R. Aaij *et al.*, *The LHCb trigger and its performance in 2011*, JINST **8** (2013) P04022, arXiv:1211.3055.

[46] T. Sjöstrand, S. Mrenna, and P. Skands, *A brief introduction to PYTHIA 8.1*, Comput. Phys. Commun. **178** (2008) 852, arXiv:0710.3820.

[47] I. Belyaev *et al.*, *Handling of the generation of primary events in Gauss, the LHCb simulation framework*, J. Phys. Conf. Ser. **331** (2011) 032047.

[48] D. J. Lange, *The EvtGen particle decay simulation package*, Nucl. Instrum. Meth. **A462** (2001) 152.

[49] P. Golonka and Z. Was, *PHOTOS Monte Carlo: A precision tool for QED corrections in Z and W decays*, Eur. Phys. J. **C45** (2006) 97, arXiv:hep-ph/0506026.

[50] Geant4 collaboration, J. Allison *et al.*, *Geant4 developments and applications*, IEEE Trans. Nucl. Sci. **53** (2006) 270; Geant4 collaboration, S. Agostinelli *et al.*, *Geant4: A simulation toolkit*, Nucl. Instrum. Meth. **A506** (2003) 250.

[51] M. Clemencic *et al.*, *The LHCb simulation application, Gauss: Design, evolution and experience*, J. Phys. Conf. Ser. **331** (2011) 032023.

[52] LHCb collaboration, R. Aaij *et al.*, *Study of the kinematic dependences of Λ_b^0 production in pp collisions and a measurement of the $\Lambda_b^0 \to \Lambda_c^+ \pi^-$ branching fraction*, JHEP **08** (2014) 143, arXiv:1405.6842.

[53] Particle Data Group, M. Tanabashi *et al.*, *Review of particle physics*, Phys. Rev. **D98** (2018) 030001.

[54] V. V. Gligorov and M. Williams, *Efficient, reliable and fast high-level triggering using a bonsai boosted decision tree*, JINST **8** (2013) P02013, arXiv:1210.6861.

[55] M. Feindt, *A neural Bayesian estimator for conditional probability densities*, arXiv:physics/0402093.

[56] M. Feindt and U. Kerzel, *The NeuroBayes neural network package*, Nucl. Instrum. Meth. **A559** (2006) 190.

[57] T. Skwarnicki, *A study of the radiative cascade transitions between the Upsilon-prime and Upsilon resonances*, PhD thesis, Institute of Nuclear Physics, Krakow, 1986, DESY-F31-86-02.

[58] LHCb collaboration, R. Aaij *et al.*, *Angular moments of the decay* $\Lambda_b^0 \to \Lambda\mu^+\mu^-$, JHEP **09** (2018) 146, `arXiv:1808.00264`.

[59] M. Pivk and F. R. Le Diberder, *sPlot: A statistical tool to unfold data distributions*, Nucl. Instrum. Meth. **A555** (2005) 356, `arXiv:physics/0402083`.

[60] B. Efron, *Bootstrap methods: Another look at the jackknife*, Ann. Statist. **7** (1979) 1.

[61] N. Metropolis *et al.*, *Equation of state calculations by fast computing machines*, The Journal of Chemical Physics **21** (1953) 1087.

[62] W. K. Hastings, *Monte Carlo sampling methods using Markov chains and their applications*, Biometrika **57** (1970) 97.

LHCb collaboration

R. Aaij[31], C. Abellán Beteta[49], T. Ackernley[59], B. Adeva[45], M. Adinolfi[53], H. Afsharnia[9], C.A. Aidala[81], S. Aiola[25], Z. Ajaltouni[9], S. Akar[66], J. Albrecht[14], F. Alessio[47], M. Alexander[58], A. Alfonso Albero[44], G. Alkhazov[37], P. Alvarez Cartelle[60], A.A. Alves Jr[45], S. Amato[2], Y. Amhis[11], L. An[21], L. Anderlini[21], G. Andreassi[48], A. Andreianov[37], M. Andreotti[20], F. Archilli[16], A. Artamonov[43], M. Artuso[67], K. Arzymatov[41], E. Aslanides[10], M. Atzeni[49], B. Audurier[11], S. Bachmann[16], J.J. Back[55], S. Baker[60], V. Balagura[11,b], W. Baldini[20], J. Baptista Leite[1], R.J. Barlow[61], S. Barsuk[11], W. Barter[60], M. Bartolini[23,47,h], F. Baryshnikov[78], J.M. Basels[13], G. Bassi[28], V. Batozskaya[35], B. Batsukh[67], A. Battig[14], A. Bay[48], M. Becker[14], F. Bedeschi[28], I. Bediaga[1], A. Beiter[67], V. Belavin[41], S. Belin[26], V. Bellee[48], K. Belous[43], I. Belyaev[38], G. Bencivenni[22], E. Ben-Haim[12], S. Benson[31], A. Berezhnoy[39], R. Bernet[49], D. Berninghoff[16], H.C. Bernstein[67], C. Bertella[47], E. Bertholet[12], A. Bertolin[27], C. Betancourt[49], F. Betti[19,e], M.O. Bettler[54], Ia. Bezshyiko[49], S. Bhasin[53], J. Bhom[33], M.S. Bieker[14], S. Bifani[52], P. Billoir[12], A. Bizzeti[21,t], M. Bjørn[62], M.P. Blago[47], T. Blake[55], F. Blanc[48], S. Blusk[67], D. Bobulska[58], V. Bocci[30], O. Boente Garcia[45], T. Boettcher[63], A. Boldyrev[79], A. Bondar[42,w], N. Bondar[37,47], S. Borghi[61], M. Borisyak[41], M. Borsato[16], J.T. Borsuk[33], T.J.V. Bowcock[59], A. Boyer[47], C. Bozzi[20], M.J. Bradley[60], S. Braun[65], A. Brea Rodriguez[45], M. Brodski[47], J. Brodzicka[33], A. Brossa Gonzalo[55], D. Brundu[26], E. Buchanan[53], A. Büchler-Germann[49], A. Buonaura[49], C. Burr[47], A. Bursche[26], A. Butkevich[40], J.S. Butter[31], J. Buytaert[47], W. Byczynski[47], S. Cadeddu[26], H. Cai[72], R. Calabrese[20,g], L. Calero Diaz[22], S. Cali[22], R. Calladine[52], M. Calvi[24,i], M. Calvo Gomez[44,l], P. Camargo Magalhaes[53], A. Camboni[44,l], P. Campana[22], D.H. Campora Perez[31], A.F. Campoverde Quezada[5], L. Capriotti[19,e], A. Carbone[19,e], G. Carboni[29], R. Cardinale[23,h], A. Cardini[26], I. Carli[6], P. Carniti[24,i], K. Carvalho Akiba[31], A. Casais Vidal[45], G. Casse[59], M. Cattaneo[47], G. Cavallero[47], S. Celani[48], R. Cenci[28,o], J. Cerasoli[10], M.G. Chapman[53], M. Charles[12], Ph. Charpentier[47], G. Chatzikonstantinidis[52], M. Chefdeville[8], V. Chekalina[41], C. Chen[3], S. Chen[26], A. Chernov[33], S.-G. Chitic[47], V. Chobanova[45], S. Cholak[48], M. Chrzaszcz[33], A. Chubykin[37], V. Chulikov[37], P. Ciambrone[22], M.F. Cicala[55], X. Cid Vidal[45], G. Ciezarek[47], F. Cindolo[19], P.E.L. Clarke[57], M. Clemencic[47], H.V. Cliff[54], J. Closier[47], J.L. Cobbledick[61], V. Coco[47], J.A.B. Coelho[11], J. Cogan[10], E. Cogneras[9], L. Cojocariu[36], P. Collins[47], T. Colombo[47], A. Contu[26], N. Cooke[52], G. Coombs[58], S. Coquereau[44], G. Corti[47], C.M. Costa Sobral[55], B. Couturier[47], D.C. Craik[63], J. Crkovská[66], A. Crocombe[55], M. Cruz Torres[1,y], R. Currie[57], C.L. Da Silva[66], E. Dall'Occo[14], J. Dalseno[45,53], C. D'Ambrosio[47], A. Danilina[38], P. d'Argent[47], A. Davis[61], O. De Aguiar Francisco[47], K. De Bruyn[47], S. De Capua[61], M. De Cian[48], J.M. De Miranda[1], L. De Paula[2], M. De Serio[18,d], P. De Simone[22], J.A. de Vries[76], C.T. Dean[66], W. Dean[81], D. Decamp[8], L. Del Buono[12], B. Delaney[54], H.-P. Dembinski[14], A. Dendek[34], V. Denysenko[49], D. Derkach[79], O. Deschamps[9], F. Desse[11], F. Dettori[26,f], B. Dey[7], A. Di Canto[47], P. Di Nezza[22], S. Didenko[78], H. Dijkstra[47], V. Dobishuk[51], F. Dordei[26], M. Dorigo[28,x], A.C. dos Reis[1], L. Douglas[58], A. Dovbnya[50], K. Dreimanis[59], M.W. Dudek[33], L. Dufour[47], P. Durante[47], J.M. Durham[66], D. Dutta[61], M. Dziewiecki[16], A. Dziurda[33], A. Dzyuba[37], S. Easo[56], U. Egede[69], V. Egorychev[38], S. Eidelman[42,w], S. Eisenhardt[57], S. Ek-In[48], L. Eklund[58], S. Ely[67], A. Ene[36], E. Epple[66], S. Escher[13], J. Eschle[49], S. Esen[31], T. Evans[47], A. Falabella[19], J. Fan[3], Y. Fan[5], N. Farley[52], S. Farry[59], D. Fazzini[11], P. Fedin[38], M. Féo[47], P. Fernandez Declara[47], A. Fernandez Prieto[45], F. Ferrari[19,e], L. Ferreira Lopes[48], F. Ferreira Rodrigues[2], S. Ferreres Sole[31], M. Ferrillo[49], M. Ferro-Luzzi[47], S. Filippov[40], R.A. Fini[18], M. Fiorini[20,g], M. Firlej[34], K.M. Fischer[62], C. Fitzpatrick[61], T. Fiutowski[34], F. Fleuret[11,b], M. Fontana[47], F. Fontanelli[23,h], R. Forty[47], V. Franco Lima[59], M. Franco Sevilla[65], M. Frank[47], C. Frei[47], D.A. Friday[58], J. Fu[25,p], Q. Fuehring[14], W. Funk[47], E. Gabriel[57], T. Gaintseva[41], A. Gallas Torreira[45], D. Galli[19,e],

S. Gallorini[27], S. Gambetta[57], Y. Gan[3], M. Gandelman[2], P. Gandini[25], Y. Gao[4], L.M. Garcia Martin[46], J. García Pardiñas[49], B. Garcia Plana[45], F.A. Garcia Rosales[11], L. Garrido[44], D. Gascon[44], C. Gaspar[47], D. Gerick[16], E. Gersabeck[61], M. Gersabeck[61], T. Gershon[55], D. Gerstel[10], Ph. Ghez[8], V. Gibson[54], A. Gioventù[45], P. Gironella Gironell[44], L. Giubega[36], C. Giugliano[20,g], K. Gizdov[57], V.V. Gligorov[12], C. Göbel[70], E. Golobardes[44,l], D. Golubkov[38], A. Golutvin[60,78], A. Gomes[1,a], P. Gorbounov[38], I.V. Gorelov[39], C. Gotti[24,i], E. Govorkova[31], J.P. Grabowski[16], R. Graciani Diaz[44], T. Grammatico[12], L.A. Granado Cardoso[47], E. Graugés[44], E. Graverini[48], G. Graziani[21], A. Grecu[36], R. Greim[31], P. Griffith[20,g], L. Grillo[61], L. Gruber[47], B.R. Gruberg Cazon[62], C. Gu[3], M. Guarise[20], P. A. Günther[16], E. Gushchin[40], A. Guth[13], Yu. Guz[43,47], T. Gys[47], T. Hadavizadeh[62], G. Haefeli[48], C. Haen[47], S.C. Haines[54], P.M. Hamilton[65], Q. Han[7], X. Han[16], T.H. Hancock[62], S. Hansmann-Menzemer[16], N. Harnew[62], T. Harrison[59], R. Hart[31], C. Hasse[14], M. Hatch[47], J. He[5], M. Hecker[60], K. Heijhoff[31], K. Heinicke[14], A.M. Hennequin[47], K. Hennessy[59], L. Henry[25,46], J. Heuel[13], A. Hicheur[68], D. Hill[62], M. Hilton[61], P.H. Hopchev[48], J. Hu[16], J. Hu[71], W. Hu[7], W. Huang[5], W. Hulsbergen[31], T. Humair[60], R.J. Hunter[55], M. Hushchyn[79], D. Hutchcroft[59], D. Hynds[31], P. Ibis[14], M. Idzik[34], P. Ilten[52], A. Inglessi[37], K. Ivshin[37], R. Jacobsson[47], S. Jakobsen[47], E. Jans[31], B.K. Jashal[46], A. Jawahery[65], V. Jevtic[14], F. Jiang[3], M. John[62], D. Johnson[47], C.R. Jones[54], B. Jost[47], N. Jurik[62], S. Kandybei[50], M. Karacson[47], J.M. Kariuki[53], N. Kazeev[79], M. Kecke[16], F. Keizer[54,47], M. Kelsey[67], M. Kenzie[55], T. Ketel[32], B. Khanji[47], A. Kharisova[80], K.E. Kim[67], T. Kirn[13], V.S. Kirsebom[48], S. Klaver[22], K. Klimaszewski[35], S. Koliiev[51], A. Kondybayeva[78], A. Konoplyannikov[38], P. Kopciewicz[34], R. Kopecna[16], P. Koppenburg[31], M. Korolev[39], I. Kostiuk[31,51], O. Kot[51], S. Kotriakhova[37], P. Kravchenko[37], L. Kravchuk[40], R.D. Krawczyk[47], M. Kreps[55], F. Kress[60], S. Kretzschmar[13], P. Krokovny[42,w], W. Krupa[34], W. Krzemien[35], W. Kucewicz[33,k], M. Kucharczyk[33], V. Kudryavtsev[42,w], H.S. Kuindersma[31], G.J. Kunde[66], T. Kvaratskheliya[38], D. Lacarrere[47], G. Lafferty[61], A. Lai[26], D. Lancierini[49], J.J. Lane[61], G. Lanfranchi[22], C. Langenbruch[13], O. Lantwin[49,78], T. Latham[55], F. Lazzari[28,u], R. Le Gac[10], S.H. Lee[81], R. Lefèvre[9], A. Leflat[39,47], O. Leroy[10], T. Lesiak[33], B. Leverington[16], H. Li[71], L. Li[62], X. Li[66], Y. Li[6], Z. Li[67], X. Liang[67], T. Lin[60], R. Lindner[47], V. Lisovskyi[14], G. Liu[71], S. Liu[6], X. Liu[3], D. Loh[55], A. Loi[26], J. Lomba Castro[45], I. Longstaff[58], J.H. Lopes[2], G. Loustau[49], G.H. Lovell[54], Y. Lu[6], D. Lucchesi[27,n], M. Lucio Martinez[31], Y. Luo[3], A. Lupato[61], E. Luppi[20,g], O. Lupton[55], A. Lusiani[28,s], X. Lyu[5], S. Maccolini[19,e], F. Machefert[11], F. Maciuc[36], V. Macko[48], P. Mackowiak[14], S. Maddrell-Mander[53], L.R. Madhan Mohan[53], O. Maev[37], A. Maevskiy[79], D. Maisuzenko[37], M.W. Majewski[34], S. Malde[62], B. Malecki[47], A. Malinin[77], T. Maltsev[42,w], H. Malygina[16], G. Manca[26,f], G. Mancinelli[10], R. Manera Escalero[44], D. Manuzzi[19,e], D. Marangotto[25,p], J. Maratas[9,v], J.F. Marchand[8], U. Marconi[19], S. Mariani[21,47,21], C. Marin Benito[11], M. Marinangeli[48], P. Marino[48], J. Marks[16], P.J. Marshall[59], G. Martellotti[30], L. Martinazzoli[47], M. Martinelli[24,i], D. Martinez Santos[45], F. Martinez Vidal[46], A. Massafferri[1], M. Materok[13], R. Matev[47], A. Mathad[49], Z. Mathe[47], V. Matiunin[38], C. Matteuzzi[24], K.R. Mattioli[81], A. Mauri[49], E. Maurice[11,b], M. McCann[60], L. Mcconnell[17], A. McNab[61], R. McNulty[17], J.V. Mead[59], B. Meadows[64], C. Meaux[10], G. Meier[14], N. Meinert[74], D. Melnychuk[35], S. Meloni[24,i], M. Merk[31], A. Merli[25], L. Meyer Garcia[2], M. Mikhasenko[47], D.A. Milanes[73], E. Millard[55], M.-N. Minard[8], O. Mineev[38], L. Minzoni[20,g], S.E. Mitchell[57], B. Mitreska[61], D.S. Mitzel[47], A. Mödden[14], A. Mogini[12], R.D. Moise[60], T. Mombächer[14], I.A. Monroy[73], S. Monteil[9], M. Morandin[27], G. Morello[22], M.J. Morello[28,s], J. Moron[34], A.B. Morris[10], A.G. Morris[55], R. Mountain[67], H. Mu[3], F. Muheim[57], M. Mukherjee[7], M. Mulder[47], D. Müller[47], K. Müller[49], C.H. Murphy[62], D. Murray[61], P. Muzzetto[26], P. Naik[53], T. Nakada[48], R. Nandakumar[56], T. Nanut[48], I. Nasteva[2], M. Needham[57], I. Neri[20,g], N. Neri[25,p], S. Neubert[16], N. Neufeld[47], R. Newcombe[60], T.D. Nguyen[48], C. Nguyen-Mau[48,m], E.M. Niel[11], S. Nieswand[13], N. Nikitin[39], N.S. Nolte[47], C. Nunez[81], A. Oblakowska-Mucha[34], V. Obraztsov[43],

S. Ogilvy[58], D.P. O'Hanlon[53], R. Oldeman[26,f], C.J.G. Onderwater[75], J. D. Osborn[81], A. Ossowska[33], J.M. Otalora Goicochea[2], T. Ovsiannikova[38], P. Owen[49], A. Oyanguren[46], P.R. Pais[48], T. Pajero[28,28,47,s], A. Palano[18], M. Palutan[22], G. Panshin[80], A. Papanestis[56], M. Pappagallo[57], L.L. Pappalardo[20,g], C. Pappenheimer[64], W. Parker[65], C. Parkes[61], C.J. Parkinson[45], G. Passaleva[21,47], A. Pastore[18], M. Patel[60], C. Patrignani[19,e], A. Pearce[47], A. Pellegrino[31], M. Pepe Altarelli[47], S. Perazzini[19], D. Pereima[38], P. Perret[9], K. Petridis[53], A. Petrolini[23,h], A. Petrov[77], S. Petrucci[57], M. Petruzzo[25,p], B. Pietrzyk[8], G. Pietrzyk[48], M. Pili[62], D. Pinci[30], J. Pinzino[47], F. Pisani[19], A. Piucci[16], V. Placinta[36], S. Playfer[57], J. Plews[52], M. Plo Casasus[45], F. Polci[12], M. Poli Lener[22], M. Poliakova[67], A. Poluektov[10], N. Polukhina[78,c], I. Polyakov[67], E. Polycarpo[2], G.J. Pomery[53], S. Ponce[47], A. Popov[43], D. Popov[52], S. Poslavskii[43], K. Prasanth[33], L. Promberger[47], C. Prouve[45], V. Pugatch[51], A. Puig Navarro[49], H. Pullen[62], G. Punzi[28,o], W. Qian[5], J. Qin[5], R. Quagliani[12], B. Quintana[8], N.V. Raab[17], R.I. Rabadan Trejo[10], B. Rachwal[34], J.H. Rademacker[53], M. Rama[28], M. Ramos Pernas[45], M.S. Rangel[2], F. Ratnikov[41,79], G. Raven[32], M. Reboud[8], F. Redi[48], F. Reiss[12], C. Remon Alepuz[46], Z. Ren[3], V. Renaudin[62], S. Ricciardi[56], D.S. Richards[56], S. Richards[53], K. Rinnert[59], P. Robbe[11], A. Robert[12], A.B. Rodrigues[48], E. Rodrigues[59], J.A. Rodriguez Lopez[73], M. Roehrken[47], A. Rollings[62], V. Romanovskiy[43], M. Romero Lamas[45], A. Romero Vidal[45], J.D. Roth[81], M. Rotondo[22], M.S. Rudolph[67], T. Ruf[47], J. Ruiz Vidal[46], A. Ryzhikov[79], J. Ryzka[34], J.J. Saborido Silva[45], N. Sagidova[37], N. Sahoo[55], B. Saitta[26,f], C. Sanchez Gras[31], C. Sanchez Mayordomo[46], R. Santacesaria[30], C. Santamarina Rios[45], M. Santimaria[22], E. Santovetti[29,j], G. Sarpis[61], M. Sarpis[16], A. Sarti[30], C. Satriano[30,r], A. Satta[29], M. Saur[5], D. Savrina[38,39], L.G. Scantlebury Smead[62], S. Schael[13], M. Schellenberg[14], M. Schiller[58], H. Schindler[47], M. Schmelling[15], T. Schmelzer[14], B. Schmidt[47], O. Schneider[48], A. Schopper[47], H.F. Schreiner[64], M. Schubiger[31], S. Schulte[48], M.H. Schune[11], R. Schwemmer[47], B. Sciascia[22], A. Sciubba[22], S. Sellam[68], A. Semennikov[38], A. Sergi[52,47], N. Serra[49], J. Serrano[10], L. Sestini[27], A. Seuthe[14], P. Seyfert[47], D.M. Shangase[81], M. Shapkin[43], L. Shchutska[48], T. Shears[59], L. Shekhtman[42,w], V. Shevchenko[77], E. Shmanin[78], J.D. Shupperd[67], B.G. Siddi[20], R. Silva Coutinho[49], L. Silva de Oliveira[2], G. Simi[27,n], S. Simone[18,d], I. Skiba[20,g], N. Skidmore[16], T. Skwarnicki[67], M.W. Slater[52], J.G. Smeaton[54], A. Smetkina[38], E. Smith[13], I.T. Smith[57], M. Smith[60], A. Snoch[31], M. Soares[19], L. Soares Lavra[9], M.D. Sokoloff[64], F.J.P. Soler[58], I. Solovyev[37], B. Souza De Paula[2], B. Spaan[14], E. Spadaro Norella[25,p], P. Spradlin[58], F. Stagni[47], M. Stahl[64], S. Stahl[47], P. Stefko[48], O. Steinkamp[49,78], S. Stemmle[16], O. Stenyakin[43], M. Stepanova[37], H. Stevens[14], S. Stone[67], S. Stracka[28], M.E. Stramaglia[48], M. Straticiuc[36], D. Strekalina[78], S. Strokov[80], J. Sun[26], L. Sun[72], Y. Sun[65], P. Svihra[61], K. Swientek[34], A. Szabelski[35], T. Szumlak[34], M. Szymanski[47], S. Taneja[61], Z. Tang[3], T. Tekampe[14], F. Teubert[47], E. Thomas[47], K.A. Thomson[59], M.J. Tilley[60], V. Tisserand[9], S. T'Jampens[8], M. Tobin[6], S. Tolk[47], L. Tomassetti[20,g], D. Torres Machado[1], D.Y. Tou[12], E. Tournefier[8], M. Traill[58], M.T. Tran[48], E. Trifonova[78], C. Trippl[48], A. Tsaregorodtsev[10], G. Tuci[28,o], A. Tully[48], N. Tuning[31], A. Ukleja[35], A. Usachov[31], A. Ustyuzhanin[41,79], U. Uwer[16], A. Vagner[80], V. Vagnoni[19], A. Valassi[47], G. Valenti[19], M. van Beuzekom[31], H. Van Hecke[66], E. van Herwijnen[47], C.B. Van Hulse[17], M. van Veghel[75], R. Vazquez Gomez[44], P. Vazquez Regueiro[45], C. Vázquez Sierra[31], S. Vecchi[20], J.J. Velthuis[53], M. Veltri[21,q], A. Venkateswaran[67], M. Veronesi[31], M. Vesterinen[55], J.V. Viana Barbosa[47], D. Vieira[64], M. Vieites Diaz[48], H. Viemann[74], X. Vilasis-Cardona[44,l], E. Vilella Figueras[59], G. Vitali[28], A. Vitkovskiy[31], A. Vollhardt[49], D. Vom Bruch[12], A. Vorobyev[37], V. Vorobyev[42,w], N. Voropaev[37], R. Waldi[74], J. Walsh[28], J. Wang[3], J. Wang[72], J. Wang[6], M. Wang[3], Y. Wang[7], Z. Wang[49], D.R. Ward[54], H.M. Wark[59], N.K. Watson[52], D. Websdale[60], A. Weiden[49], C. Weisser[63], B.D.C. Westhenry[53], D.J. White[61], M. Whitehead[53], D. Wiedner[14], G. Wilkinson[62], M. Wilkinson[67], I. Williams[54], M. Williams[63,69], M.R.J. Williams[61], T. Williams[52], F.F. Wilson[56], W. Wislicki[35], M. Witek[33], L. Witola[16], G. Wormser[11],

S.A. Wotton[54], H. Wu[67], K. Wyllie[47], Z. Xiang[5], D. Xiao[7], Y. Xie[7], H. Xing[71], A. Xu[4], J. Xu[5], L. Xu[3], M. Xu[7], Q. Xu[5], Z. Xu[4], Z. Yang[3], Z. Yang[65], Y. Yao[67], L.E. Yeomans[59], H. Yin[7], J. Yu[7], X. Yuan[67], O. Yushchenko[43], K.A. Zarebski[52], M. Zavertyaev[15,c], M. Zdybal[33], M. Zeng[3], D. Zhang[7], L. Zhang[3], S. Zhang[4], Y. Zhang[47], A. Zhelezov[16], Y. Zheng[5], X. Zhou[5], Y. Zhou[5], X. Zhu[3], V. Zhukov[13,39], J.B. Zonneveld[57], S. Zucchelli[19,e], G. Zunica[61].

[1] *Centro Brasileiro de Pesquisas Físicas (CBPF), Rio de Janeiro, Brazil*
[2] *Universidade Federal do Rio de Janeiro (UFRJ), Rio de Janeiro, Brazil*
[3] *Center for High Energy Physics, Tsinghua University, Beijing, China*
[4] *School of Physics State Key Laboratory of Nuclear Physics and Technology, Peking University, Beijing, China*
[5] *University of Chinese Academy of Sciences, Beijing, China*
[6] *Institute Of High Energy Physics (IHEP), Beijing, China*
[7] *Institute of Particle Physics, Central China Normal University, Wuhan, Hubei, China*
[8] *Univ. Grenoble Alpes, Univ. Savoie Mont Blanc, CNRS, IN2P3-LAPP, Annecy, France*
[9] *Université Clermont Auvergne, CNRS/IN2P3, LPC, Clermont-Ferrand, France*
[10] *Aix Marseille Univ, CNRS/IN2P3, CPPM, Marseille, France*
[11] *Université Paris-Saclay, CNRS/IN2P3, IJCLab, Orsay, France*
[12] *LPNHE, Sorbonne Université, Paris Diderot Sorbonne Paris Cité, CNRS/IN2P3, Paris, France*
[13] *I. Physikalisches Institut, RWTH Aachen University, Aachen, Germany*
[14] *Fakultät Physik, Technische Universität Dortmund, Dortmund, Germany*
[15] *Max-Planck-Institut für Kernphysik (MPIK), Heidelberg, Germany*
[16] *Physikalisches Institut, Ruprecht-Karls-Universität Heidelberg, Heidelberg, Germany*
[17] *School of Physics, University College Dublin, Dublin, Ireland*
[18] *INFN Sezione di Bari, Bari, Italy*
[19] *INFN Sezione di Bologna, Bologna, Italy*
[20] *INFN Sezione di Ferrara, Ferrara, Italy*
[21] *INFN Sezione di Firenze, Firenze, Italy*
[22] *INFN Laboratori Nazionali di Frascati, Frascati, Italy*
[23] *INFN Sezione di Genova, Genova, Italy*
[24] *INFN Sezione di Milano-Bicocca, Milano, Italy*
[25] *INFN Sezione di Milano, Milano, Italy*
[26] *INFN Sezione di Cagliari, Monserrato, Italy*
[27] *INFN Sezione di Padova, Padova, Italy*
[28] *INFN Sezione di Pisa, Pisa, Italy*
[29] *INFN Sezione di Roma Tor Vergata, Roma, Italy*
[30] *INFN Sezione di Roma La Sapienza, Roma, Italy*
[31] *Nikhef National Institute for Subatomic Physics, Amsterdam, Netherlands*
[32] *Nikhef National Institute for Subatomic Physics and VU University Amsterdam, Amsterdam, Netherlands*
[33] *Henryk Niewodniczanski Institute of Nuclear Physics Polish Academy of Sciences, Kraków, Poland*
[34] *AGH - University of Science and Technology, Faculty of Physics and Applied Computer Science, Kraków, Poland*
[35] *National Center for Nuclear Research (NCBJ), Warsaw, Poland*
[36] *Horia Hulubei National Institute of Physics and Nuclear Engineering, Bucharest-Magurele, Romania*
[37] *Petersburg Nuclear Physics Institute NRC Kurchatov Institute (PNPI NRC KI), Gatchina, Russia*
[38] *Institute of Theoretical and Experimental Physics NRC Kurchatov Institute (ITEP NRC KI), Moscow, Russia, Moscow, Russia*
[39] *Institute of Nuclear Physics, Moscow State University (SINP MSU), Moscow, Russia*
[40] *Institute for Nuclear Research of the Russian Academy of Sciences (INR RAS), Moscow, Russia*
[41] *Yandex School of Data Analysis, Moscow, Russia*
[42] *Budker Institute of Nuclear Physics (SB RAS), Novosibirsk, Russia*
[43] *Institute for High Energy Physics NRC Kurchatov Institute (IHEP NRC KI), Protvino, Russia, Protvino, Russia*
[44] *ICCUB, Universitat de Barcelona, Barcelona, Spain*
[45] *Instituto Galego de Física de Altas Enerxías (IGFAE), Universidade de Santiago de Compostela,*

Santiago de Compostela, Spain
[46] *Instituto de Fisica Corpuscular, Centro Mixto Universidad de Valencia - CSIC, Valencia, Spain*
[47] *European Organization for Nuclear Research (CERN), Geneva, Switzerland*
[48] *Institute of Physics, Ecole Polytechnique Fédérale de Lausanne (EPFL), Lausanne, Switzerland*
[49] *Physik-Institut, Universität Zürich, Zürich, Switzerland*
[50] *NSC Kharkiv Institute of Physics and Technology (NSC KIPT), Kharkiv, Ukraine*
[51] *Institute for Nuclear Research of the National Academy of Sciences (KINR), Kyiv, Ukraine*
[52] *University of Birmingham, Birmingham, United Kingdom*
[53] *H.H. Wills Physics Laboratory, University of Bristol, Bristol, United Kingdom*
[54] *Cavendish Laboratory, University of Cambridge, Cambridge, United Kingdom*
[55] *Department of Physics, University of Warwick, Coventry, United Kingdom*
[56] *STFC Rutherford Appleton Laboratory, Didcot, United Kingdom*
[57] *School of Physics and Astronomy, University of Edinburgh, Edinburgh, United Kingdom*
[58] *School of Physics and Astronomy, University of Glasgow, Glasgow, United Kingdom*
[59] *Oliver Lodge Laboratory, University of Liverpool, Liverpool, United Kingdom*
[60] *Imperial College London, London, United Kingdom*
[61] *Department of Physics and Astronomy, University of Manchester, Manchester, United Kingdom*
[62] *Department of Physics, University of Oxford, Oxford, United Kingdom*
[63] *Massachusetts Institute of Technology, Cambridge, MA, United States*
[64] *University of Cincinnati, Cincinnati, OH, United States*
[65] *University of Maryland, College Park, MD, United States*
[66] *Los Alamos National Laboratory (LANL), Los Alamos, United States*
[67] *Syracuse University, Syracuse, NY, United States*
[68] *Laboratory of Mathematical and Subatomic Physics , Constantine, Algeria, associated to* [2]
[69] *School of Physics and Astronomy, Monash University, Melbourne, Australia, associated to* [55]
[70] *Pontifícia Universidade Católica do Rio de Janeiro (PUC-Rio), Rio de Janeiro, Brazil, associated to* [2]
[71] *Guangdong Provencial Key Laboratory of Nuclear Science, Institute of Quantum Matter, South China Normal University, Guangzhou, China, associated to* [3]
[72] *School of Physics and Technology, Wuhan University, Wuhan, China, associated to* [3]
[73] *Departamento de Fisica , Universidad Nacional de Colombia, Bogota, Colombia, associated to* [12]
[74] *Institut für Physik, Universität Rostock, Rostock, Germany, associated to* [16]
[75] *Van Swinderen Institute, University of Groningen, Groningen, Netherlands, associated to* [31]
[76] *Universiteit Maastricht, Maastricht, Netherlands, associated to* [31]
[77] *National Research Centre Kurchatov Institute, Moscow, Russia, associated to* [38]
[78] *National University of Science and Technology "MISIS", Moscow, Russia, associated to* [38]
[79] *National Research University Higher School of Economics, Moscow, Russia, associated to* [41]
[80] *National Research Tomsk Polytechnic University, Tomsk, Russia, associated to* [38]
[81] *University of Michigan, Ann Arbor, United States, associated to* [67]

[a] *Universidade Federal do Triângulo Mineiro (UFTM), Uberaba-MG, Brazil*
[b] *Laboratoire Leprince-Ringuet, Palaiseau, France*
[c] *P.N. Lebedev Physical Institute, Russian Academy of Science (LPI RAS), Moscow, Russia*
[d] *Università di Bari, Bari, Italy*
[e] *Università di Bologna, Bologna, Italy*
[f] *Università di Cagliari, Cagliari, Italy*
[g] *Università di Ferrara, Ferrara, Italy*
[h] *Università di Genova, Genova, Italy*
[i] *Università di Milano Bicocca, Milano, Italy*
[j] *Università di Roma Tor Vergata, Roma, Italy*
[k] *AGH - University of Science and Technology, Faculty of Computer Science, Electronics and Telecommunications, Kraków, Poland*
[l] *DS4DS, La Salle, Universitat Ramon Llull, Barcelona, Spain*
[m] *Hanoi University of Science, Hanoi, Vietnam*
[n] *Università di Padova, Padova, Italy*
[o] *Università di Pisa, Pisa, Italy*
[p] *Università degli Studi di Milano, Milano, Italy*
[q] *Università di Urbino, Urbino, Italy*

[r] *Università della Basilicata, Potenza, Italy*
[s] *Scuola Normale Superiore, Pisa, Italy*
[t] *Università di Modena e Reggio Emilia, Modena, Italy*
[u] *Università di Siena, Siena, Italy*
[v] *MSU - Iligan Institute of Technology (MSU-IIT), Iligan, Philippines*
[w] *Novosibirsk State University, Novosibirsk, Russia*
[x] *INFN Sezione di Trieste, Trieste, Italy*
[y] *Universidad Nacional Autonoma de Honduras, Tegucigalpa, Honduras*